THE DEVELOPMENT OF A FATIGUE TEST MACHINE TO INVESTIGATE THE FUNCTIONAL FATIGUE LIFE OF HIGH TEMPERATURE SHAPE MEMORY ALLOYS AND THE DETERMINATION OF THE FUNCTIONAL FATIGUE LIFE OF THESE ALLOYS

YÜKSEK SICAKLIK ŞEKİL HAFIZALI ALAŞIMLARIN FONKSİYONEL YORULMA ÖMÜRLERİNİ İNCELEMEK ÜZERE FONKSİYONEL YORULMA TEST CİHAZI GELİŞTİRİLMESİ VE BU ALAŞIMLARIN FONKSİYONEL YORULMA ÖMÜRLERİNİN TAYİNİ

HASAN HÜSEYİN SAYGILI

DOÇ. DR. BENAT KOÇKAR
Supervisor

Submitted to Graduate School of Science and Engineering of Hacettepe University
as a Partial Fulfillment to the Requirements
for the Award of the Degree of Master of Sciences
in Mechanical Engineering

2018

This work named **"The Development of a Fatigue Test Machine to Investigate the Functional Fatigue Life of High Temperature Shape Memory Alloys and the Determination of the Functional Fatigue Life of These Alloys"** by **HASAN HÜSEYİN SAYGILI** has been approved as a thesis for the degree of **MASTER OF SCIENCE IN MECHANICAL ENGINEERING** by the below mentioned Examining Committee Members.

Prof. Dr. Murat KÖKSAL
Head

Assoc. Prof. Dr. Benat KOÇKAR
Supervisor

Assist. Prof. Dr.-Ing. Okan GÖRTAN
Member

Assist.Prof. Dr. Bilsay SÜMER
Member

Assoc. Prof. Dr. Kadri Can ATLI
Member

This thesis has been approved as a thesis for the degree of **MASTER OF SCIENCE IN MECHANICAL ENGINEERING** by a Board of Directors of the Institute for Graduate School of Science and Engineering.

Prof. Dr. Menemşe GÜMÜŞDERELİOĞLU

Director of the Institute of
Graduate School of Science and Engineering

YAYINLAMA VE FİKRİ MÜLKİYET HAKLARI BEYANI

Enstitü tarafından onaylanan lisansüstü tezimin/raporumun tamamını veya herhangi bir kısmını, basılı (kağıt) ve elektronik formatta arşivleme ve aşağıda verilen koşullarla kullanıma açma iznini Hacettepe üniversitesine verdiğimi bildiririm. Bu izinle Üniversiteye verilen kullanım hakları dışındaki tüm fikri mülkiyet haklarım bende kalacak, tezimin tamamının ya da bir bölümünün gelecekteki çalışmalarda (makale, kitap, lisans ve patent vb.) kullanım hakları bana ait olacaktır.

Tezin kendi orijinal çalışmam olduğunu, başkalarının haklarını ihlal etmediğimi ve tezimin tek yetkili sahibi olduğumu beyan ve taahhüt ederim. Tezimde yer alan telif hakkı bulunan ve sahiplerinden yazılı izin alınarak kullanması zorunlu metinlerin yazılı izin alarak kullandığımı ve istenildiğinde suretlerini Üniversiteye teslim etmeyi taahhüt ederim.

☐ **Tezimin/Raporumun tamamı dünya çapında erişime açılabilir ve bir kısmı veya tamamının fotokopisi alınabilir.**
(Bu seçenekle teziniz arama motorlarında indekslenebilecek, daha sonra tezinizin erişim statüsünün değiştirilmesini talep etseniz ve kütüphane bu talebinizi yerine getirse bile, tezinin arama motorlarının önbelleklerinde kalmaya devam edebilecektir.)

☑ **Tezimin/Raporumun 11/06/2021 tarihine kadar erişime açılmasını ve fotokopi alınmasını (İç Kapak, Özet, İçindekiler ve Kaynakça hariç) istemiyorum.**
(Bu sürenin sonunda uzatma için başvuruda bulunmadığım taktirde, tezimin/raporumun tamamı her yerden erişime açılabilir, kaynak gösterilmek şartıyla bir kısmı ve ya tamamının fotokopisi alınabilir)

☐ **Tezimin/Raporumun .... tarihine kadar erişime açılmasını istemiyorum, ancak kaynak gösterilmek şartıyla bir kısmı veya tamamının fotokopisinin alınmasını onaylıyorum.**

☐ **Serbest Seçenek/Yazarın Seçimi**
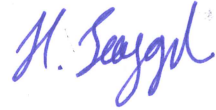
06/07/2018

(İmza)

Hasan Hüseyin Saygılı

ETHICS

In this thesis study, prepared in accordance with the spelling rules of Institute of Graduate Studies in Science of Hacettepe University,

I declare that

- all the information and documents have been obtained in the base of the academic rules
- all audio-visual and written information and results have been presented according to the rules of scientific ethics
- in case of using others Works, related studies have been cited in accordance with the scientific standards
- all cited studies have been fully referenced
- I did not do any distortion in the data set
- and any part of this thesis has not been presented as another thesis study at this or any other university.

11.06.2018

HASAN HÜSEYİN SAYGILI

ABSTRACT

THE DEVELOPMENT OF A FATIGUE TEST MACHINE TO INVESTIGATE THE FUNCTIONAL FATIGUE LIFE OF HIGH TEMPERATURE SHAPE MEMORY ALLOYS AND THE DETERMINATION OF THE FUNCTIONAL FATIGUE LIFE OF THESE ALLOYS

Hasan Hüseyin SAYGILI

Master of Sciences, Department of Mechanical Engineering

Supervisor: Assist. Prof. Dr. Benat KOÇKAR

June 2018, 72 Pages

Shape memory alloys are special materials which can be utilized as actuators for several applications. Their high power to weight ratio draws attention to many applications, especially in aerospace industry. Most of the applications require multiple actuation and transformation temperatures which are above the 100ºC. Thus, stability of shape memory alloys in terms of actuation strain and transformation temperatures are very important in order to define the feasibility of using shape memory alloys for industrial applications. Aging is a one of the methods for Nickel rich NiTi alloys that adjust the transformation temperatures and enhance the cyclic stability of the shape memory alloys. In this study, $Ni_{50.3}Ti_{29.7}Hf_{20}$ high temperature shape memory alloy was used since it is one of the most promising high temperature shape memory alloy in terms of high transformation temperatures as well as high strength.

The functional fatigue properties of the extruded and aged $Ni_{50.3}Ti_{29.7}Hf_{20}$ high temperature shape memory alloy were investigated in order to reveal the effect of aging on functional fatigue behavior. Material was produced using high purity Ni, Ti and Hf elements via

i

vacuum induction melting under high purity argon atmosphere, then placed in a mild steel can for hot extrusion at 900°C with an area reduction of 4:1. One batch of the material was aged at 550°C for 3 hours and one batch of material was used in the experiments in the extruded condition. Same experiments were conducted on both of the materials for comparison. Stress-free transformation temperatures were measured using Perkin Elmer Differential Scanning Calorimetry (DSC) 800. Load-biased heating and cooling experiments were conducted by UTEST 50 kN servo-mechanical test machine with embedded heating and cooling systems. These experiments were done to determine the stress magnitude under which the samples showed the first irrecoverable strain. Functional fatigue experiments were performed on custom-built functional fatigue test setup. Post-mortem optical microscope investigations after functional fatigue tests were performed to investigate the crack propagation during the fatigue experiments. Transmission electron microscopy was also conducted before functional fatigue tests to determine the twin and precipitate structures and the oxide particles in the matrix.

Stress-free transformation temperatures were increased above 100°C after aging heat treatment at 550°C for 3 hours, as expected. It was also found that aging at 550°C for 3 hours led to an increase in critical stress for slip such that the first irrecoverable strain was determined under 600 MPa stress level while extruded sample showed irrecoverable strain under 300 MPa in load-biased heating-cooling experiments. Therefore, 200 MPa stress magnitude was chosen as the threshold stress level since no irrecoverable strain was detected for extruded and aged samples and the functional fatigue experiments were conducted under 200 MPa constant stress level. The sample aged at 550°C for 3 hours exhibited considerably better stability during functional fatigue experiments with respect to the extruded one. The decrease in actuation strain values of the aged sample through 16534th cycles was smaller than that of the extruded sample. The test was stopped at this point because fracture was experienced. On the other hand, extruded sample lost its actuation strain before 5000th cycle and therefore, test was ceased. Transmission electron microscopy investigations revealed that oxide particles are in the matrix, thus these oxide particles might be one the reasons of fracture since they may act as the crack initiation points at the beginning of the functional fatigue experiments.

ÖZET

YÜKSEK SICAKLIK ŞEKİL HAFIZALI ALAŞIMLARIN FONKSİYONEL YORULMA ÖMÜRLERİNİ İNCELEMEK ÜZERE FONKSİYONEL YORULMA TEST CİHAZI GELİŞTİRİLMESİ VE BU ALAŞIMLARIN FONKSİYONEL YORULMA ÖMÜRLERİNİN TAYİNİ

Hasan Hüseyin SAYGILI

Yüksek Lisans, Makina Mühendisliği Bölümü

Tez Danışmanı: Doç. Dr. Benat KOÇKAR

Haziran 2018, 72 Sayfa

Şekil hafızalı alaşımlar çeşitli uygulamalarda eyleyici olarak kullanılabilen özel materyellerdir. Sahip oldukları yüksek güç/ağırlık oranı özellikle havacılık alanı olmak üzere birçok alanda dikkat çekmektedir. Uygulamaların birçoğu çoklu tahrik ve 100ºC'nin üzerinde yüksek dönüşüm sıcaklıkalarının olmasını gerektirmektedir. Bu nedenle, şekil hafızalı alaşımların endüstriyel uygulamarının uygunluğunun tanımlanmasında, eyleyici gerinimi ve dönüşüm sıcaklıkları açısından kararlılık çok önemlidir. Yaşlandırma işlemi Nikelce zengin NiTi alaşımlarında dönüşüm sıcaklıklarını ayarlamak ve çevrimsel kararlılığı arttırmak için kullanılan yöntemlerden biridir. Bu çalışmada, sahip olduğu yüksek dönüşüm sıcaklığının yanı sıra yüksek dayanımı açısından en umut verici yüksek sıcaklık şekil hafızalı alaşımlarından biri olan $Ni_{50.3}Ti_{29.7}Hf_{20}$ yüksek sıcaklık şekil hafızalı alaşımı kullanılmıştır.

Ekstrüde halde ve yaşlandırılmış $Ni_{50.3}Ti_{29.7}Hf_{20}$ yüksek sıcaklık şekil hafızalı alaşımının fonksiyonel yorulma özellikleri, yaşlandırma işleminin fonksiyonel yorulma davranışına

etkisini ortaya koymak üzere incelenmiştir. Malzeme yüksek saflıktaki Ni, Ti ve Hf elemenleri kullanılarak vakum indüksiyonla eritme yoluyla yüksek saflıktaki argon atmosferi altında üretilmiştir. Sonrasında yumuşak çelik ile kaplanarak 4:1 oranında alan indirgemesi olacak şekilde 900ºC'de sıcak ekstrüzyona tabi tutulmuştur. Bir grup malzemenin 550ºC'de yaşlandırma işlemi yapılırken ve bir grup malzeme deneylerde ekstrude halde kullanılmıştır. Karşılaştırma yapılabilmesi için yaşlandırılmış ve ekstrüde haldeki malzemelere aynı deneyler uygulanmıştır. Yüksüz dönüşüm sıcaklıkları Perkin Elmer Differential Scanning Calorimetry (DSC) 800 kullanılarak ölçülmüştür. Sabit yük altında ısıtma ve soğutma deneyleri ısıtma ve soğutma sistemleri yerleştirilmiş UTEST 50 kN servo-mekanik test makinasında gerçekleştirilmiştir. Bu testler malzemelerin ilk hangi gerilim değeri altında geri kazanılamayan gerinim gösterdiklerini saptamak için gerçekleştirilmiştir. Fonksiyonel yorulma deneyleri özel üretim fonksiyonel yorulma test cihazında yapılmıştır. Fonksiyonel yorulma deneyi sonrası optik mikroskop incelemesi yorulma deneyleri sırasındaki çatlak ilerlemesini incelemek üzere gerçekleştirilmiştir. Aynı zamanda geçirmeli elektron mikroskobu incelemesi de fonksiyonel yorulma testleri öncesinde matristeki ikizlenme ve çökelti yapıları ile oksit parçacıklarını belirlemek için yapılmıştır.

Yüksüz dönüşüm sıcaklıkları 550ºC'de 3 saat yaşlandırmanın ardından beklenildiği gibi 100ºC'nin üzerine çıkmıştır. Aynı zamanda 550ºC'de 3 saat yaşlandırma ile kayma için kritik gerilim değeri artmıştır. Öyle ki yük altında ısıtma – soğutma deneylerinde ekstürüde örnekte ilk geri kazanılamayan gerinim 300 MPa yük altında görülürken yaşlandırılmış örnekte 600 MPa yük altında görülmüştür. Bu nedenle 200 MPa gerilim değeri, ekstrüde ve yaşlandırılmış örneklerde geri kazanılamayan gerinim göstermediğinden sınır değeri olarak belirlenmiş ve fonksiyonel yorulma deneyleri 200 MPa yük altında gerçekleştirilmiştir. 550ºC'de 3 saat yaşlandırılmış örnek ekstürüde örneğe göre fonksiyonel yorulma testlerinde kayda değer seviyede daha iyi çevrimsel kararlılık göstermiştir. Yaşlandırılmış örnekte 16534 çevrim boyunca eyleyici geriniminde azalma ekstrüde örnekten daha azdır. Test bu noktada kopma gerçekleştiği için durdurulmuştur. Diğer taraftan ekstürüde örnek 5000 çevrimden önce eyleyici gerinimini kaybetmiştir ve bu nedenle test durdurulmuştur. Geçirmeli elektron mikroskobu incelemesi sonucunda matriste oksit parçacıkları bulunmuştur. Bu parçacıklar çatlak başlangıç noktası olarak davranabildikleri için fonksiyonel yorulma testlerindeki kopmanın nedeni olabilirler.

Anahtar kelimeler: Yüksek Sıcaklık Şekil Hafızalı Alaşımları, Fonksiyonel Yorulma, Yaşlandırma, Dönüşüm Sıcaklıkları, Eyleyici Gerinimi

ACKNOWLEDGEMENTS

TABLE OF CONTENTS

LIST OF TABLES

LIST OF FIGURES

SYMBOLS AND ABBREVIATIONS

Abbreviations:

A_f	:	Austenite finish temperature
A_s	:	Austenite start temperature
M_f	:	Martensite finish temperature
M_s	:	Martensite start temperature
DSC	:	Differential Scanning Calorimetry
TEM	:	Transmission Electron Microscopy
SMA	:	Shape Memory Alloy
HTSMA	:	High Temperature Shape Memory Alloy
LPDS	:	Linear Potentiometric Displacement Sensor
Ni	:	Nickel
Ti	:	Titanium
Hf	:	Hafnium

1   INTRODUCTION

Shape memory alloys (SMA) are very unique and special materials with the ability of remembering their original shape after they have been deformed. When SMA is deformed in martensite phase, twinned martensitic structure transforms to detwinned structure. If SMA is heated to high temperature (austenite) phase, it recovers this shape change. This recovery can take place under high stress levels with noticeable strain magnitudes, which provides high power to weight ratio. These unique properties of SMAs lead to use them as actuators in many fields, especially in aerospace applications.

Most applications of SMAs require multiple actuation cycles. Therefore, it is necessary to maintain the actuation stability. This stability can be explained as no or very small changes in transformation temperatures and actuation strain values. The term of functional fatigue refers to the investigation of the change in these properties of SMAs with the number of cycles.

Many studies have been conducted on binary Ni-Ti SMAs, since they have good cyclic stability, high actuation strain and good mechanical properties [1–3] . However, their martensitic transformation temperatures are lower than 100°C such that the usage of these materials are limited for most the applications in aerospace industry. Controlling the actuation behavior of SMAs at high temperatures which requires higher transformation temperatures has attracted a great attention recently. The SMAs which are utilized for high temperature applications are categorized as "High Temperature Shape Memory Alloys" (HTSMAs) if their transformation temperatures are above 100°C.

Adding a ternary alloying element to Ni-Ti based SMAs is one of the methods for the development of HTSMAs. Au, Pt, Pd, Zr and Hf are used to produce HTSMAs as additional alloying elements in NiTi binary systems [4–7]. However, Au, Pt and Pd are not suitable for commercial applications since their costs are relatively high than that of the others. Thus, studies are focused on Zr and Hf addition in last decades. High oxygen affinity and brittleness of Zr makes Hf the most promising additional alloying element in Ni-Ti systems [6–11].

In Ni-rich NiTiHf HTSMAs, nano-scale precipitates can be formed via aging. These nano-scale precipitates strengthen the matrix via inhibiting the dislocation motion, so critical stress for slip increases. This increase leads to the formation of less plastic deformation

even huge stress levels are applied [10]. Nano-scale precipitates have two distinct effects on transformation temperatures. First one is the increase of the transformation temperatures with the formation of the Ni-rich precipitates which leads to the decrease of the Ni-content in the matrix. The second one is the stress field around the nano-precipitates which leads to an increase in the undercooling for complete martensitic transformation and, thus, a decrease in the transformation temperatures is observed. Therefore, it can be concluded that precipitate size and amount are very important parameters for tailoring the transformation temperatures. If precipitate size is large and volume fraction is relatively higher, first effect is dominant. If precipitate size is small and volume fraction of precipitates is low, second effect becomes dominant and transformation temperatures decreases [9, 12, 13].

$Ni_{50.3}Ti_{29.7}Hf_{20}$ HTSMA is one of the most widely studied HTSMAs, since the transformation temperatures can be adjusted precisely via precipitation hardening [5, 14, 15]. In addition to that, high critical stress for slip magnitude via aging makes $Ni_{50.3}Ti_{29.7}Hf_{20}$ the most promising HTSMA [16]. Previous studies have shown that aging 3 hours below $500^{o}C$ leads to a decrease in transformation temperatures. However, aging 3 hours above $500^{o}C$ increases the transformation temperatures. Aging $Ni_{50.3}Ti_{29.7}Hf_{20}$ alloy at $550^{o}C$ for 3 hours gives optimum results in the literature if the magnitude of the transformation temperatures and cyclic stability behaviors are considered [13].

There are lots of studies on $Ni_{50.3}Ti_{29.7}Hf_{20}$ HTSMAs such as load biased heating and cooling tests, stress free transformation behavior and microstructural investigations [17]. However, the effect of aging on functional fatigue properties of $Ni_{50.3}Ti_{29.7}Hf_{20}$ HTSMAs has not been demonstrated yet. First and only study on fatigue behavior of $Ni_{50.3}Ti_{29.7}Hf_{20}$ HTSMA is conducted and published by Karakoc and his group [18]. However, the main focus in that study was to show the effect of upper cycle temperature (UTC) on functional fatigue response of $Ni_{50.3}Ti_{29.7}Hf_{20}$ aged sample at $550^{o}C$ for 3 hours.

On the other hand, this study is about showing the effect of aging $Ni_{50.3}Ti_{29.7}Hf_{20}$ HTSMA via following the aforementioned optimum aging parameters and comparing the functional fatigue behavior of the extruded and aged samples in terms of actuation strain and transformation temperature stability. Therefore, this study has an importance with being the first study which reveals the enhancement of functional fatigue properties via aging for $Ni_{50.3}Ti_{29.7}Hf_{20}$ HTSMA. The functional fatigue tests were performed both on the extruded and the aged $Ni_{50.3}Ti_{29.7}Hf_{20}$ samples. From this point, extruded sample of $Ni_{50.3}Ti_{29.7}Hf_{20}$

16

HTSMA will be referred as "extruded" while the $Ni_{50.3}Ti_{29.7}Hf_{20}$ sample which was exposed to aging at 550°C for 3 hours after extrusion will be referred as "aged" throughout the text.

The functional fatigue investigations of shape memory alloys require cycles at the order of thousands. Cycle time is very important, since investigation of functional fatigue behavior of alloys may take years which is not practical if cycle time is long. Therefore, there is a necessity to reach high heating and cooling rates during functional fatigue test. In accordance with this purpose, a custom-built functional fatigue test setup was developed in order to investigate the functional fatigue life and cyclic stability of HTSMAs.

2   THEORY

SMAs are the alloys that showing thermoelastic martensitic transformations. They are named as SMAs, since they have an ability of remembering their original shape after they have been deformed. This remembering their shape takes place if they are heated up to certain temperature point. They have a great attraction since they have high power density, damping ratio, strength and fatigue behavior. Especially their high power density provides using these alloys as an actuator [1].

Austenite and martensite phases of SMA have single type crystal structure, however martensite phase can have two types of configurations, which are twinned martensite and detwinned martensite. If no load is applied to the SMA during martensitic transformations, twinned martensite structure takes place. If there are external loads, detwinned martensitic structure takes place. Fraction of detwinned martensitic structure increases with the increase of applied load. It should be noted that, there is no significant shape change occurs while twinned martensitic structure takes place, while macroscopic shape chance occurs during detwinned martensitic transformations [19].
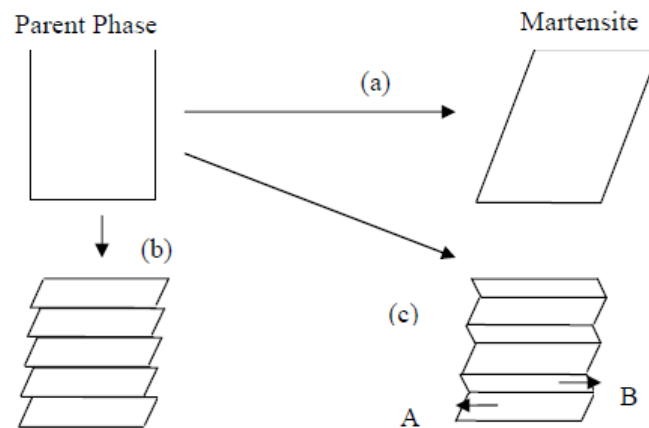
Figure 2-1: Schematic illustration of austenite, twinned martensite (c) and detwinned martensite stuctures (b) [1]

There are two unique properties of SMAs which are named as shape memory effect and superelasticity. If SMA is below the M_f temperature and it is deformed, it can recover this deformation if it is heated above the A_f temperature. This phenomenon explains the shape memory effect. If SMA is above the A_f temperature and deformed with the external load, it returns to the original shape after the load is removed [20]. It should be noted that, this deformation is not only elastic deformation and can results high strain values.

To use SMAs as actuators, some parameters are important to determine feasibility of usage SMAs as an actuator; such as transformation temperatures, hysteresis, actuation (transformation) strain, irrecoverable strain. Figure 2.1-2 represents the typical shape memory strain-temperature response of SMAs under constant load.
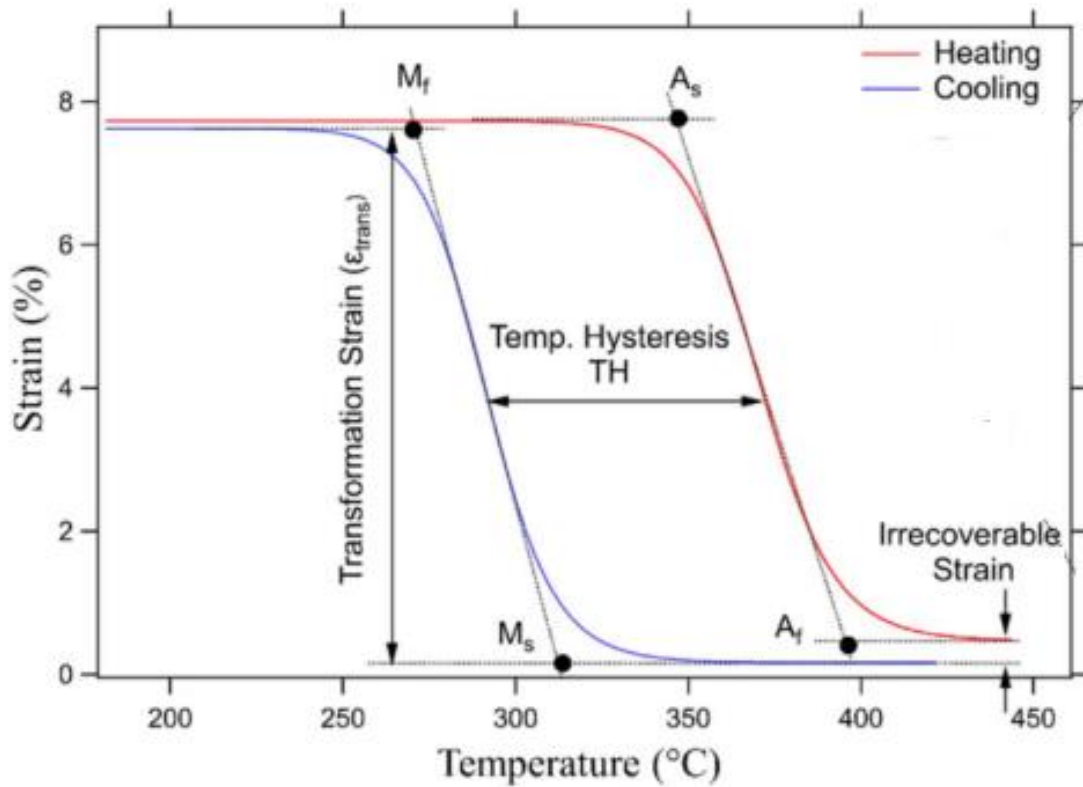
Figure 2.1-2: Stress strain curve of SMA [1]

When the material is at austenite phase and constant load is applied, the austenitic structure is elastically deformed. It should be noted that Figure 2.1-2 does not present the loading path. Figure 2.1-2 starts after loading. When the material is started to be cooled down in the presence of load, the material starts to transform to martensitic structure after critical temperature point, which is called martensite start temperature (M_s). The material continues to transform to the martensitic structure, which is accompanied by the deformation. This transformation continues until critical temperature point, where all austenitic structures transforms to martensitic structures, which is called martensite finish temperature (Mf). There is no macroscopic shape change after that point (if thermal expansion is neglected). When the material starts to heat, it begins to transform austenitic structure after critical temperature, which is called austenite start (A_s) temperature and continues to transform until it reaches to austenite finish (A_f) temperature. After that point,

all structure is austenite. The shape recovery, which provides SMAs use as an actuator occurs during this austenitic transformation. This shape recovery strain of SMA called actuation strain or transformation strain. Actuation strain is not equal to deformation strain always. If plastic deformation occurs during deformation process, SMA is not able to recover the plastic deformation. In this case, SMA recovers only recoverable deformation. However, the plastic strain which is called irrecoverable strain is retain in the material. Also, it should be noted that heating and cooling paths are not same, since dissipation of the elastic stored energy and friction during austenite to martensite and martensite to austenite transformations. The hysteresis defines the difference between the heating and cooling curves.

Defining exact point of transformation temperature is not possible. Thus, the tangent line method is used to define the transformation temperatures. The intersection points on the lines give corresponding transformation temperatures. The hysteresis on the other hand, is calculated based on the temperature difference at the middle point of actuation strain for heating and cooling curves.

These parameters of SMAs are very important, if SMAs are desired to be used as actuators. More actuation strain and higher loads generally desired in order to get high work output / volume (or mass) ratio. Beside this, transformation temperatures are also very important considering the working area of the SMAs. Most engineering applications require the working temperatures as room temperature or slightly above. Considering the temperature change of environment, transformation temperatures of SMA which is close to the room temperature is not preferred. This is because, change in working environment temperatures can cause unintended actuation of SMAs. For most applications, it is desired to have transformation temperatures above 100ºC.

2.1   Conventional Shape Memory Alloys:

2.1.1   Cu-based Shape Memory Alloys:

Most and well-known Cu-based SMAs are Cu-Zn and Cu-Al. Transformation temperatures of Cu-Zn SMA are below -50ºC where transformation temperatures of Cu-Al SMA are above 100ºC. However, wide range of transformation temperatures can be achieved via adding ternary alloying element to these alloys. Cu-Zn-Al, Cu-Al-Ni and Cu-Al-Mn are most studied Cu-based ternary SMA system. Their shape memory effect and

superelasticity properties are better than NiTi-based SMAs. However, their low cyclic stability limits the use of these alloys.

Resistance to grain boundary fracture is very important for Cu-based SMAs mechanical properties. Cu-Zn SMAs are very ductile materials and their resistance to grain boundary fracture are relatively higher than the other Cu-based SMAs. However, their transformation temperatures are very low. Adding aluminum (Al) can increase the transformation temperatures up to 100°C. However, Cu-Zn-Al SMAs are unstable above 130°C and this behavior limits their usage on industrial applications [19, 21].

2.1.2   Fe-based Shape Memory Alloys:

Fe-based SMAs have advantage of being cheaper, comparing to the NiTi-based SMAs. However, their shape memory properties are lower than Cu-based and NiTi-based SMAs. Also, their high hysteresis value limits their application area.

Fe-based SMAs can be categorized in two groups: First group consists of Fe-Pt, Fe-Pd and Fe-Ni-Co-Ti SMAs. Their hysteresis values are below 10°C. Fe-Ni-C and Fe-Mn-Si constitute of second group of Fe-based SMAs. They have large hysteresis around 150°C. Fe-Mn-Si has mechanical properties of similar to stainless steel. Thus, it has commercial application area [22].

Fe-Mn-Si SMAs are the most promising Fe-based SMA systems that adopted to the the industry. Adding Cr, Ni or Co as ternary alloying elements to Fe-Mn-Si SMA system has been studied to enhance the mechanical properties. Fe-Mn-Si SMAs can show one-way shape memory effect. However, they do not show two-way shape memory effect and superelasticity because of the high thermal hysteresis.

2.1.3   NiTi-based Shape Memory Alloys:

NiTi- based SMAs are most known and studied SMAs since they have superior shape memory characteristics. They owe their popularity to their high ductility and corrosion resistance. Also, their recovery ability makes them very attractive among conventional shape memory alloys [23].

Transformation temperatures of NiTi-based SMAs are below the 100°C. Their transformation temperatures are highly dependent on Ni content on the matrix and

thermomechanical treatments. It is known that decrease in Ni content results increase in transformation temperatures for Ni-rich SMAs. Thus, aging heat treatment is one of the method that increase the transformation temperatures of NiTi-based SMAs.

Besides other precipitates, Ti_3Ni_4 precipitates are very important to tailor the shape memory characteristic of NiTi-based SMAs. Ti_3Ni_4 precipitates which are formatted during aging process cause depletion of Ni content on matrix and result increase in transformation temperatures. Also, these precipitates limit the martensite-austenite transformation, which results less dislocation formation and stabilize the transformation [24–26].

2.2   High Temperature Shape Memory Alloys (HTSMAs):

Thermomechanical treatments on NiTi binary SMAs have limited effects on transformation temperatures. Their transformation temperatures can be increased, but transformation temperatures which are above the 100ºC cannot be achieved.

Ternary alloying element addition to NiTi-based SMAs is most promising way to increase the transformation temperatures. Effect of Au, Pt, Pd, Zr and Hf addition to NiTi-based shape memory alloys were widely studied in literature [4, 5, 9, 27, 28]. Since Au, Pt and Pd are relatively expensive materials, their use in commercial applications are limited. Thus, most studies are focused on addition of Zr and Hf to NiTi-based SMAs. However, high oxygen affinity of Zr results brittleness in HTSMAs and limits the usage of this material. Also, work output value of NiTiHf are higher than NiTiPd and NiTiPt HTSMAs (Figure 2.2-1). Due to these reasons, NiTiHf ternary alloys are widely studied as most promising HTSMAs [7, 9, 32, 10, 12, 13, 16, 18, 29–31].
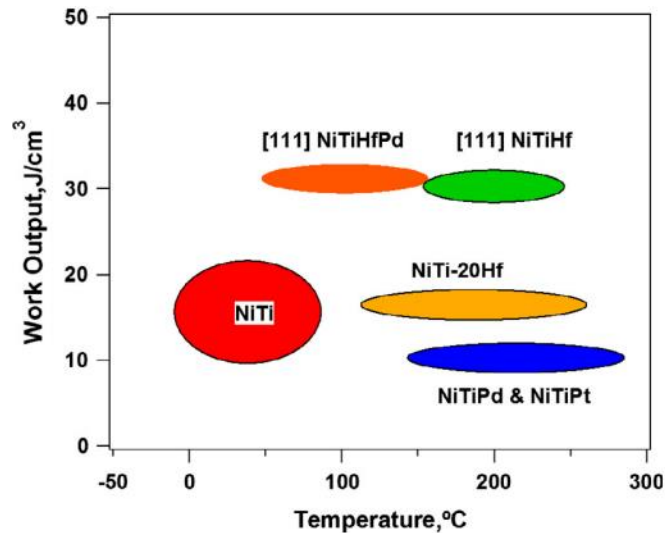
Figure 2.2-1: Work output of SMAs [13]

2.3   NiTiHf HTSMAs:

Effect of Hf content in NiTiHf HTSMAs was first investigated by Potapov et al [33]. The study where Ni lean HTSMAs were used investigate the effect of Hf content. It revelas that increase in Hf content results increase in transformation temperatures. For example, Mf-Af transformation range which was $50^{\circ}C$-$142^{\circ}C$ for 8% Hf content increased to $127^{\circ}C$-$276^{\circ}C$ with 20% Hf content. Bessghini et al addresses the effect of Ti+Hf content on material properties. It is reported that increase in Ti+Hf content makes the material more brittle. This study also shows that Ti+Hf content does not affect the transformation temperatures much [34].

Further studies focused on Ni-rich NiTiHf HTMAs. It was demonstrated that formation of precipitates increases the transformation temperatures and transformation temperature stability on Ni-rich NiTiHf HTMAs [35]. Effect of precipitation was investigated in detail by Karaca et al. $Ni_{50,3}Ti_{29,7}Hf_{20}$ HTSMA material was aged with different temperatures at the range of $300^{\circ}C$-$900^{\circ}C$ [13]. The stress-free transformation curves of aged materials can be seen in Figure 2.3-1.
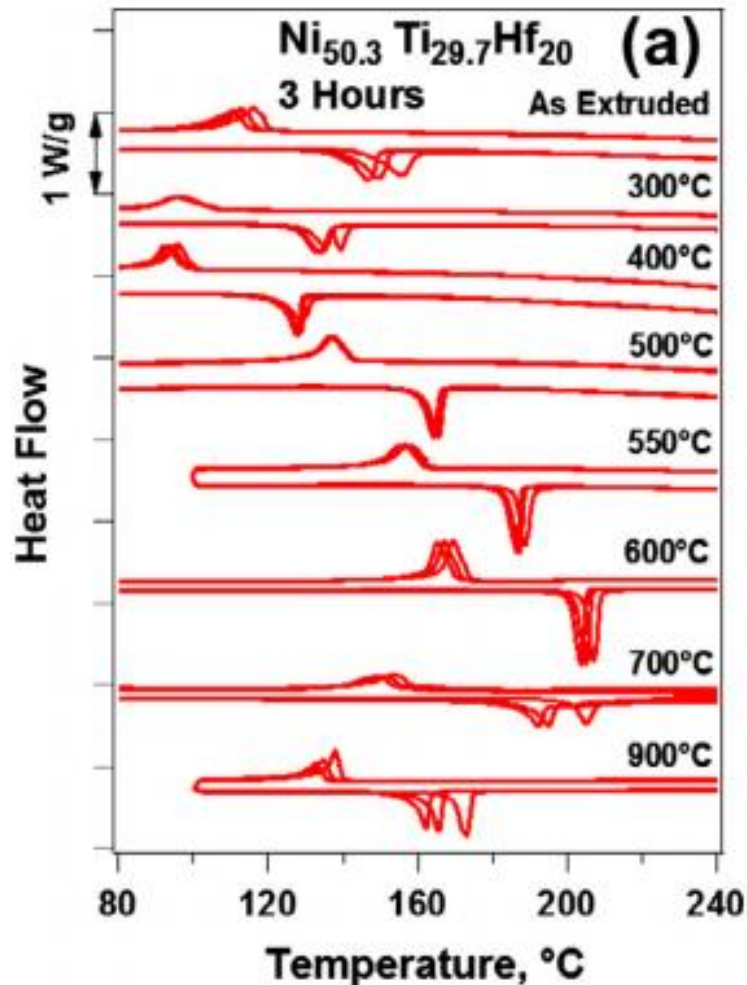
Figure 2.3-1: Stress free transformation curves of $Ni_{50,3}Ti_{29,7}Hf_{20}$ HTSMA for different aging temperatures [13]

It can be concluded that aging temperatures below 500°C results in a decrease in transformation temperatures. On the other hand, aging temperatures 500°C and above increases the transformation temperatures. It can be explained with the two effect of precipitation on tailoring the transformation temperatures. First effect bases on the stress fields around the precipitates. This stress fields repress the martensitic transformation, therefore overcooling become necessary for martensitic transformation. This situation results decrease in transformation temperatures. On the other hand, depletion of Ni from matrix results increase in transformation temperatures, which can be explained with the effect of Ni content on matrix. Since the decrease in Ni content on matrix results increase in transformation temperatures, depletion of Ni from matrix via aging causes increase in transformation temperatures. For the aging below 500°C, first effect become dominant because the precipitation volume fractions are small. Increase in aging temperatures results

24

increase in volume fraction of precipitates. Therefore, second effect become dominant and increase in transformation temperatures is observed [36].

2.4   Functional Fatigue of SMAs

There are limited studies on functional fatigue studies for SMAs. Early studies were conducted on NiTi binary SMAs. Effect of rolling direction was studied on Ni-rich NiTi SMAs. It was found that actuation strain and fatigue life of the SMA are highly dependent on rolling direction. Maximum fatigue life was observed with 0.9% actuation strain and approximately 40000 cycles under 200 MPa functional fatigue tests [37].

Agboola et al. investigated the functional fatigue life of Ni-rich $Ni_{60}Ti_{40}$ SMA under different constant stress levels. It was found that maximum fatigue life was observed under 100 MPa stress level and 0.6% actuation strain up to 68987 cycles. On the other hand, minimum fatigue life was observed under 250 MPa stress level with 2.23% actuation strain up to 1500 cycles [38].

However, there is only one study about functional fatigue life of HTMAs. This study focuses on the effect of upper cycle temperature (UCT) on functional fatigue life of $Ni_{50,3}Ti_{29,7}Hf_{20}$ HTSMA which was aged at 550ºC for 3 hours. The tests which were conducted on different stress levels and with different UCTs shows that UCT has a negative effect on fatigue life of HTSMAs. The increase in UCT is accompanied with an increase in actuation strain leads more expansion and contraction of cracks which promotes crack propagation. Other effect of UCT can be considered as decreasing the strength of the material at relatively higher temperatures, which results early failure.   Maximum life was achieved under 300 MPa stress level with 250ºC UCT. However, a significant amount of loss is observed in actuation strain [18].
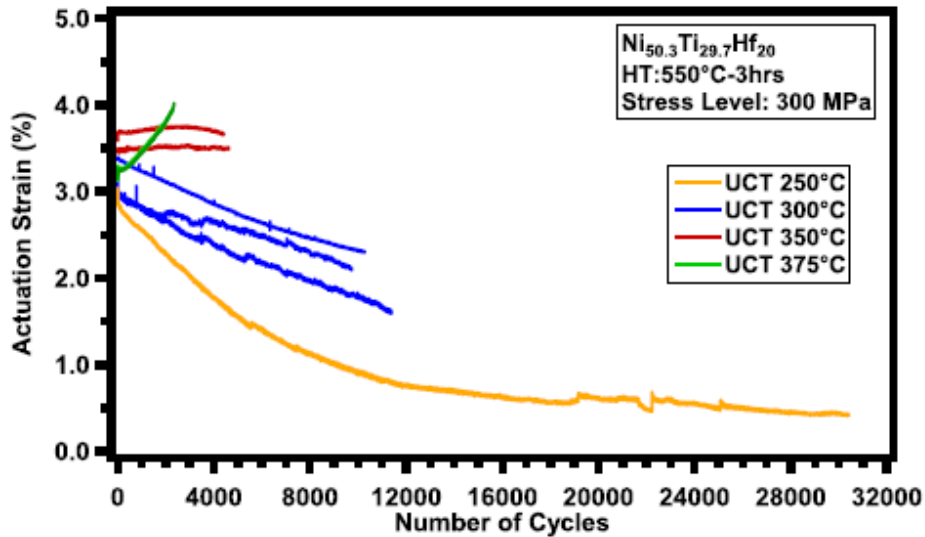
Figure 2.4-1: Actuation strain of HTSMA with respect to number of cycles for different UCTs [18]

It was also conducted that accumulation of irrecoverable strain values increased with the stress level and UCT. The highest irrecoverable strain observed for 400 MPa stress level with 350°C UCT and sample fractured before 2000th cycle. On the other hand, 300 MPa stress level with 300°C UCT showed the least irrecoverable strain. The sample cycled more than 10000 cycles before fracture.
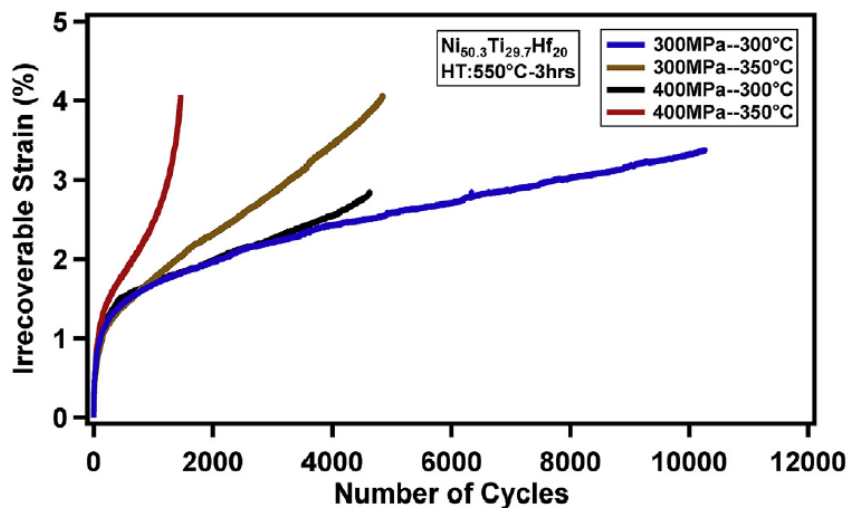
Figure 2.4-2: Irrecoverable strain with respect to number of cycles for diffent stress levels and UCTs [18]

3 EXPERIMENTAL PROCEDURES

3.1 As-received Material

High purity elemental materials of Ni, Ti and Hf were used to produce $Ni_{50.3}Ti_{29.7}Hf_{20}$ HTSMA via vacuum induction melting under high purity argon atmosphere. The material was then hot extruded at 900°C with an area reduction of 4:1 after it was sealed in mild steel can to decrease the friction between the extrusion die and the material and to prevent the oxidation during hot extrusion process. Mild steel can was removed via turning process after hot extrusion. The picture of hot extruded material can be seen Figure 3.1-1.

Figure 3.1-1. $Ni_{50.3}Ti_{29.7}Hf_{20}$ alloy after hot extrusion.

3.2 Aging Heat Treatment

Extruded samples were aged under high purity argon atmosphere at different aging temperatures, which were 450°C, 500°C and 550°C for 3 hours in order to reveal the effect

of aging temperature on transformation temperatures. Materials were wrapped in tantalum foil, which was 25.4 μm in thickness to diminish oxidation during aging heat treatments. The samples were aged in a vertical cylindrical furnace and then the samples were water quenched.

The precipitates which were formed during aging process have a major effect on transformation temperatures. The precipitation size, precipitation shape and distance between the precipitates influence the transformation behavior on matrix, which leads to change in transformation temperatures and cyclic stability [13]. The effect of aging parameters, and the precipitate properties have already known and summarized in Theory section. However, it was investigated one more time, since material properties may change from one batch to another.

3.3   Sample Preparation

Tensile specimens in flat dog bone shape with a gage length of 16.6 mm, a width of 2.25 mm and thickness of 1 mm were cut using wire electrical discharge machining (Figure 3.6-2), for both load-biased heating-cooling and functional fatigue experiments from hot extruded bulk material. Differential scanning calorimetry (DSC) and optical microscope specimens were cut via diamond saw precision cutter without applying load and at a very low speed to prevent inducing stress.

Samples for optical investigations were mechanically ground with increasing the grid size starting from 120 papers and were polished with the paper having grit size 2000. Samples were etched utilizing the solution 10% HF, 60% HNO_3 and %30 CH_3COOH (at vol.), after they were further polished with 6 μm and 1 μm alumina polishing slurries, respectively. TEM samples were prepared via utilizing focused ion beam equipment for thinning the samples down to 10-20 nm.

3.4   Differential Scanning Calorimetry

Stress-free transformation temperatures of extruded $Ni_{50.3}Ti_{29.7}Hf_{20}$ and aged $Ni_{50.3}Ti_{29.7}Hf_{20}$ samples at different temperatures were measured using Perkin Elmer Differential Scanning Calorimetry (DSC) 800 before load-biased heating-cooling and fatigue experiments. $Ni_{50.3}Ti_{29.7}Hf_{20}$ extruded and aged samples were cycled in the range of

-50°C and 350°C in order to ensure complete martensitic transformations. The heating and cooling rates during DSC experiments were kept constant at 10°C/min for all samples. $Ni_{50.3}Ti_{29.7}Hf_{20}$ alloy has been studied before and there are publications which are showing the transformation temperatures in the literature [9, 13]. However, it has been already known that the small compositional differences from batch to batch can lead to small changes in the transformation properties of the shape memory alloys. Therefore, DSC experiments were also conducted before fatigue experiments in this study.

3.5   Load-biased Heating and Cooling Tests

Load biased heating-cooling experiments were first performed using UTEST 50 kN servo-mechanical test machine. Tensile specimens were mounted to the grips and then heated above A_f temperature via conduction through the grips by resistive heaters. The tensile specimens were loaded to constant stress level, then cooled below to M_f temperature using water flowing through the copper tubing wrapped around the grips. Sample were heated and cooled under constant stress levels. After each heating-cooling cycle the stress level was increased with a magnitude 100 MPa, starting with 100 MPa stress level up to 600 MPa stress level. The sample temperatures were measured using a J type thermocouple which was attached to the gage section of the samples. The heating and cooling rates during the load-biased experiments were kept constant at 10°C/min and controlled via Autonics TM4 controller. The feedback temperature was measured via the J type thermocouples attached to the grips. The axial strain was measured with an Epsilon high temperature extensometer having ceramic extension rods attached directly to the gage of the samples. The image of test setup was presented in Figure 3.5-1. The load-biased heating-cooling experiments were conducted before fatigue experiments to determine the threshold stress level at which the first irrecoverable strain was observed. The strain-temperature curves obtained from load-biased experiments and the actuation, irrecoverable strain magnitudes together with the transformation temperatures gathered from each cycles were presented schematically at Figure 2.1-2. Load-biased heating and cooling tests performed only on extruded samples and aged samples at 550°C for 3 hours, since it had better cyclic stability and transformation temperature ranges comparing to other aging temperatures.

Figure 3.5-1. Load Biased Heating Cooling Test Setup

3.6 Functional Fatigue Test Machine Development

Custom-build functional fatigue test machine was developed in order to investigate the functional fatigue behavior of high temperature shape memory alloys. Cyclic heating and cooling were performed with the application of the constant load to the samples. The load was applied via dead weights which were hanged at the bottom of the sample. Since the number of cycles was on the order of thousands, the Joule heating method was utilized in order to reach high heating rates. Also, cooling was performed via forced air convection method to obtain high cooling rates. During the cycles, temperature, displacement and number of cycle data were collected.

Functional fatigue test machine consists of the following components:

- Aluminum sigma profile
- Direct Current (DC) power supply
- Fatigue test sample
- Sample holder heads (top and bottom)
- Linear Potentiometric Displacement Sensor (LPDS)
- Infrared pyrometer
- Air regulator

- Air nozzles
- Weights
- Data acquisition device
- Computer
- Software

Schematic drawing of the functional fatigue test setup is shown in Figure 3.6-1 and the necessary information about the aforementioned components of the setup are given below
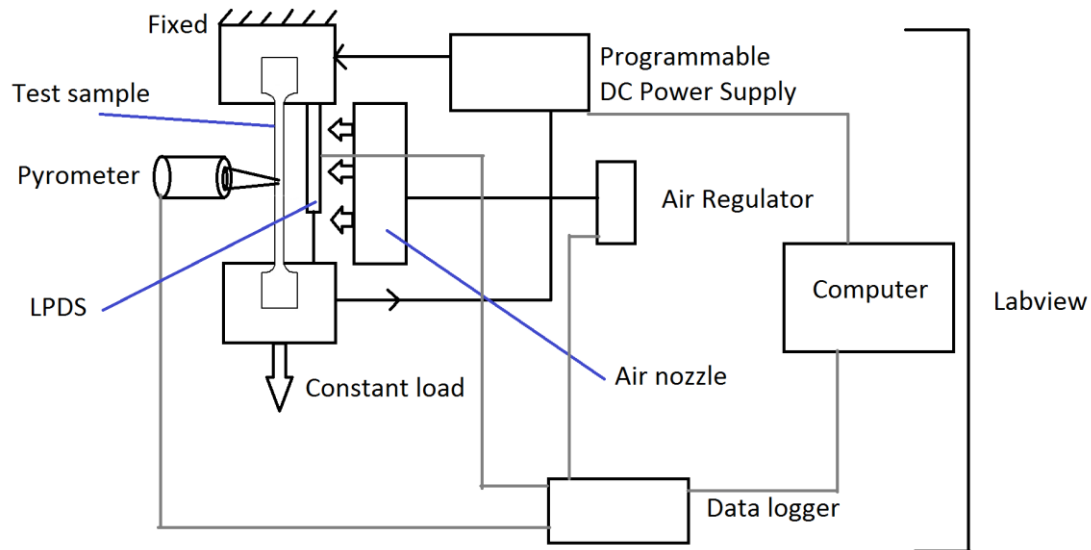
Figure 3.6-1 The Schematic Drawing of Functional Fatigue Test Setup.

3.6.1 Aluminum sigma profile:

Aluminum sigma profiles with the dimension of 45 mm x 45 mm was used to build up the structure of the test machine These sigma profiles are widely used due to their ease of construction ability with the groove structure. Additionally, sigma profiles were used in order to assemble the sensors and nozzles.

3.6.2 DC Power Supply:

Electrical current which was used in order to heat the samples (Joule heating method) was supplied by the programmable DC power supply. The amount of current or voltage can be adjusted in order to achieve desired heating rate. Also, current can be cut off to get higher cooling rate during cooling process.

The power supply is Keysight N5742A with the maximum voltage of 8 V and maximum current of 90 A. Device is working with 240 V AC current and can be connected to computer via GPIB, LAN and USB. DC output was preferred in order to eliminate the unknown effect of AC heating.

3.6.3   Fatigue Test Sample

Fatigue samples with the dog bone shape were used to investigate the functional fatigue behavior of NiTiHf samples. The samples have 16.6 mm gage length, 2.25 mm width and 1 mm thickness. Detailed drawing of test sample was illustrated at Figure 3.6-2.
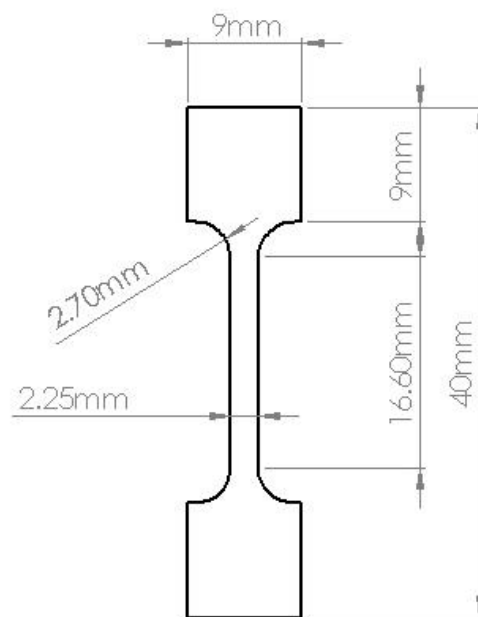
Figure 3.6-2 The Functional Fatigue Test Sample Schematic

3.6.4   Grips

There are two grips at which the test samples were attached. The edges of the test sample were cut with a certain radius and the grips were designed to hold the samples from these edges (Figure 3.6-2) such that the maximum stress values were transferred to the gage length of the sample. Top grip held the sample and attached it to aluminum sigma profile while bottom grip allowed to hang the constant loads. Also, negative and positive poles of DC power supply were attached to the top and bottom grips, thus electrical current was flown trough the samples. Hot work tool steels were used to produce the top grip and

bottom grip which were necessary for higher strength and stiffness at high working temperatures. Technical drawings of the grips are shown in (Figure 3.6-3)
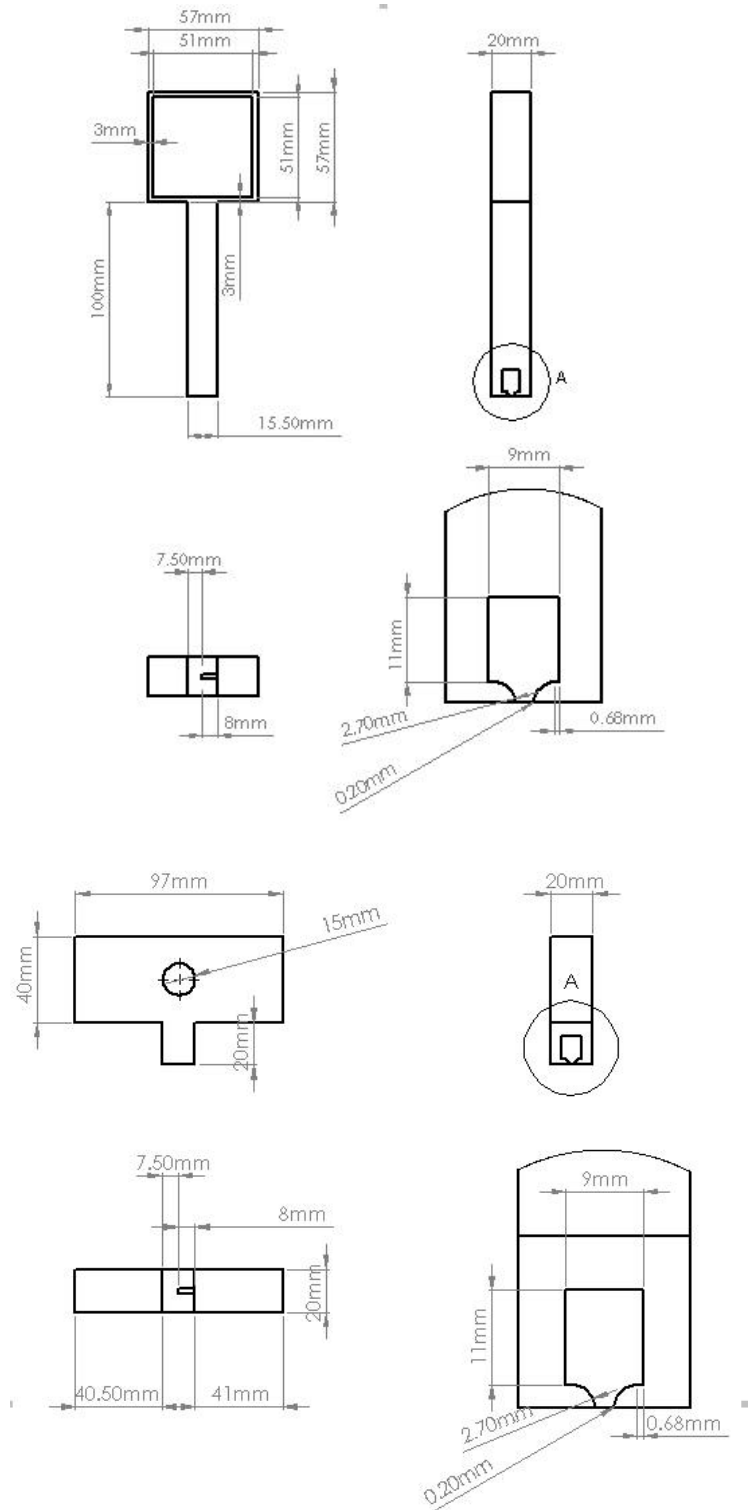
Figure 3.6-3 Technical Drawings of the Top and Bottom Grips.

3.6.5 Linear Potentiometric Displacement Sensor (LPDS)

Linear potentiometric displacement sensors (LPDSs) are the sensors that are utilized for measuring the displacement. Sensor gives output according applied voltage in the manner that the output and displacement are linearly dependent. For example; if the supply voltage is 10 V, sensor gives 10 V at maximum displacement, 0 V at 0 displacement and 5 V at the half of the its stroke. UTGM-060 (Novotechnik TR-010) LPDS was used in order to measure the displacement of the test sample during functional fatigue tests. Sensor has a stroke of 10 mm and ±0.002 sensivity. It has a spring coupled device, thus it returns to the 0 position when it is released.

3.6.6 Infrared Pyrometer

Infrared pyrometers are the temperature sensors which provide contact-free temperature measurements. They measure the thermal radiation of the object and transform it to a temperature value. Since the heating and cooling rates are high during the functional fatigue tests, it is not feasible to measure the temperature with the methods which require contact with the test sample, such as thermocouples since the response of the thermocouple types of contact sensors is very slow with these heating-cooling rates.

Optris CTlaser LTF-CF1 infrared thermometer was used with the 1.4 mm focus length at 70 mm distance in the functional fatigue test setup, considering the test samples width. It has a temperature measurement range of -50°C to +975°C and its own logger, which is supported with 24 VDC. The thermal radiation which comes from the test sample is detected by the infrared pyrometer and translated to a temperature value at the logger, then corresponding voltage value is sent to the NI data logger card at the range of 0 V-10 V.

Thermal emissivity of the test sample is an important parameter, since temperature value is translated at the logger according to thermal emissivity. However, thermal emissivity value of NiTiHf shape memory alloy is not known. Thus, test samples surface was painted with the high temperature black paint and emissivity value was set to 0.95 which was the emissivity value of the black paint. Since the paint layer on the test sample was very thin, it was assumed that temperatures of the test sample and the paint were almost equal. Hereby, the temperature of the samples was measured.

3.6.7 Air Regulator:

In order to control the cooling rate of the sample during functional fatigue tests, A digital electro-pneumatic regulator was integrated to functional fatigue test setup. CKD EVD-1000 series digital electro-pneumatic regulator was used. The power voltage of digital electro-pneumatic regulator is 24 V and it has the ability to control the air pressures up to 9 bar. Control signal was between 0 V-10 V, which was supplied by the data acquisition device.

3.6.8 Air Nozzles

Since the fatigue test samples were long and thin, air nozzles which could spray the air with a thin flow pattern were utilized in order to use the air efficiently. It has air injection section with 40 mm long, which is sufficient for cooling the samples gage length, also the grip section which is closer to the samples. Two air nozzles with the 45° angle with the test sample surface and 90° to each other were assembled to the fatigue test setup.

3.6.9 Weights

Dead weights were used in order to generate constant stress levels, which were hanged to the bottom grip. 2.5 kg, 5 kg, 10 kg and 20 kg plates were used. The weight of dead weights of bottom grip, weight platform and connection equipment were measured. The necessary weight was calculated in order to generate the target stress level. The necessary weight was hanged in the manner that the total of weights and dead weights was equal to the target weight.

3.6.10 Data Acquisition Device

National Instruments USB-6003 Multifunction input and output device was used as a data acquisition device. It has 8 analog inputs, 13 digital input/output and 2 analog output channels. Sensor outputs were measured via analog input channels while the air regulator was controlled via analog output channel. Wiring with the sensors and regulator was performed with its own screw terminals. It has 0 V-10 V range for both analog input and output. Also, it has USB port for the connection to the computer.

3.6.11 Computer

The data were collected and stored by the data acquisition device via program scripted on software program by computer.

3.6.12 Software

National Instruments LabView Program was used in order to control the functional fatigue tests.

3.7 Functional Fatigue Tests

Functional fatigue experiments were performed on a custom-built functional fatigue test setup. Tensile samples were attached to the aluminum sigma profile chassis through mounting them to the grips. The weights were hanged to the bottom grip in order to generate constant stress magnitudes on the tensile samples. The material was heated with the electric current passing through sample, which was called as Joule heating method. Programmable DC power supply's negative and positive poles were connected to the grips. Temperature was measured from the mid sections of the samples' gage length with the Optris CTlaser LTF-CF1 infrared thermometer. Tensile samples were coated with high temperature black paint, since the emissivity value of the black paint was already known. Cooling was performed using compressed air which was forced to the tensile sample using an air nozzle. A digital electro-pneumatic regulator was used to control the amount of air flow. Displacement was measured with a linear potentiometric displacement sensor (LPDS). Actuation strain was calculated with difference between martensitic and austenitic strains. Measurement, control and data acquisition were performed using the program scripted on National Instruments LabView Program. National Instruments USB-6003 data logger was utilized to take data from the sensors as input and to control the proportional valve as an output device. The lower cycle and the upper cycle temperatures and the heating/cooling rate were entered manually to the program. PI controller integrated to the program controlled the electrical current passing through the sample during heating and the amount of air compressed to the sample surface during cooling in order to achieve the desired heating/cooling rate. Temperature, displacement and number of cycle data were stored to the computer.

3.8 Microstructure Evaluation

Microstructural evaluation of extruded and aged samples was first determined using Nikon Eclipse LV 150 optical microscope. Optic microscope investigation of the samples

performed before functional fatigue tests and after functional fatigue tests. Also, transmission electron microscope was used in order to determine the twin structure, precipitates and oxide particles.

Illustration of all processes was schematically described in Figure 3.8-1, Figure 3.8-2 and Figure 3.8-3.
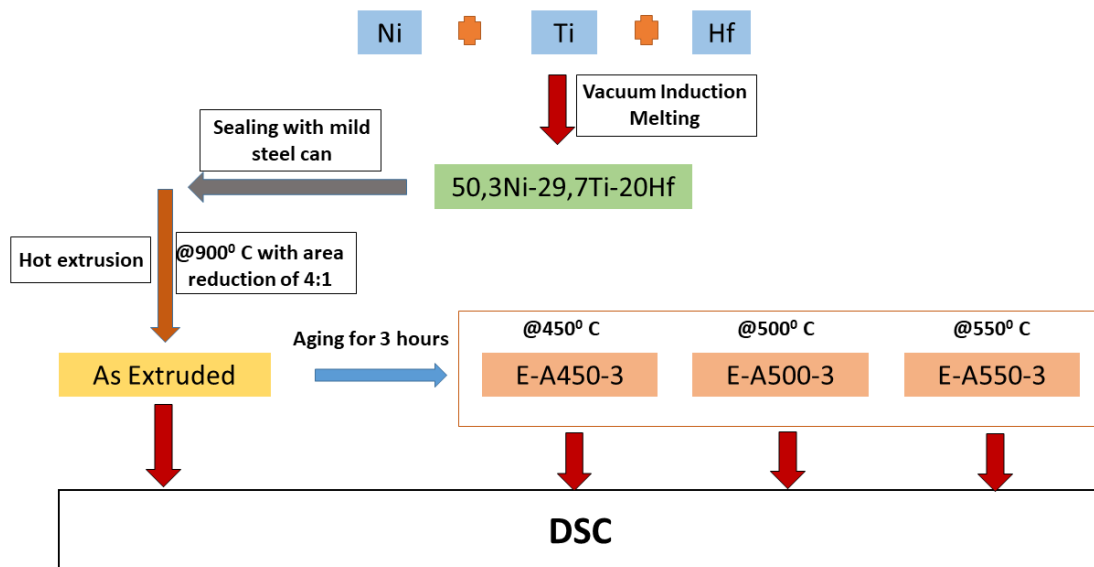

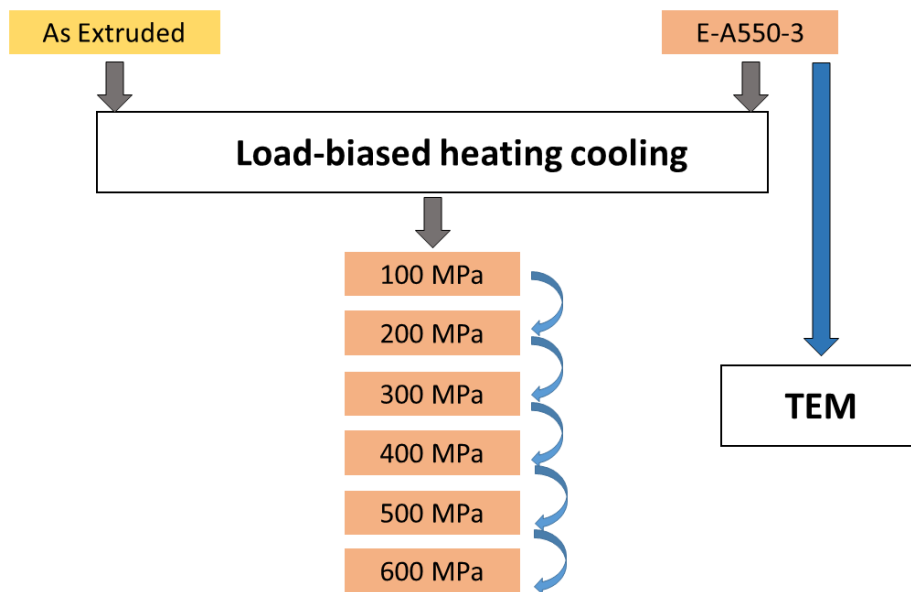Figure 3.8-1. Processes of the Material and Thermal DSC Tests

Figure 3.8-2 Load Biased Thermomechanical Tests and Transmission Electron Imaging
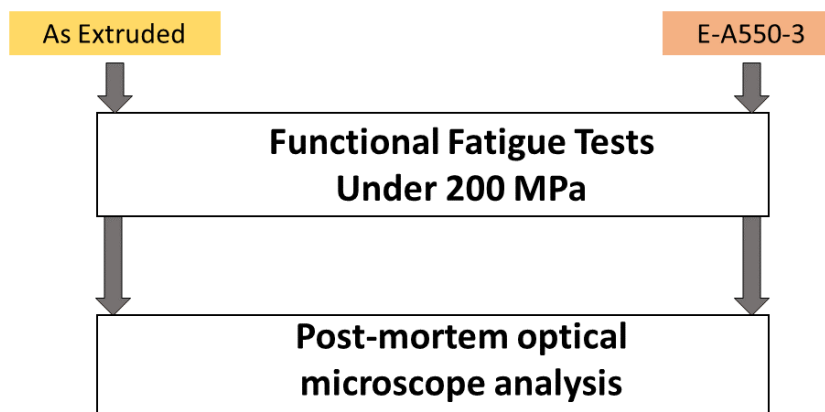
Figure 3.8-3. Fatigue Tests and Failure Analysis

4 EXPERIMENTAL RESULTS

4.1 Differential Scanning Calorimetry

Normalized heat flow vs. temperature curves from the DSC experiments of the samples which were extruded and aged at 450°C, 500°C and 550°C are represented in Figure 4.1-1. A decrease in transformation temperatures was observed after aging at 450°C since the stress field around the nano-sized precipitates suppressed the transformation such that higher undercooling became necessary for martensitic transformation. However, aging at elevated temperatures led to an increase in transformation temperatures. This can be explained with the decrease in Ni content in the matrix with the increase in volume fraction of precipitates. When the aging temperatures were increased, precipitate volume fraction became higher. Volume fraction of precipitates could be increased with the increase of the aging temperature via new precipitate nucleation or growth of existing precipitates. Also, aging time affects the volume fraction. However, 3 hours aging time kept constant for all aging temperatures in order to reveal the temperature effect.
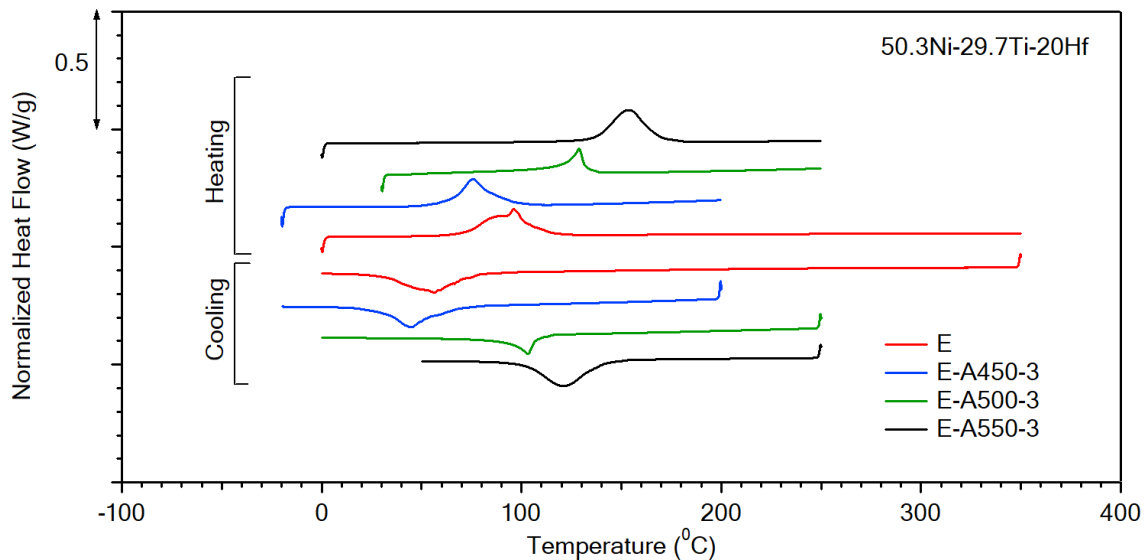
Figure 4.1-1. DSC Results For Extruded and Aged Ni$_{50.3}$Ti$_{29.7}$Hf$_{20}$ Samples

It should be noted that, Ni depletion due to precipitation formation and the stress field around the nano-sized precipitates affect the transformation temperatures in a different way. Decrease in transformation temperatures due to the stress fields around nano-sized precipitates is observed when the samples are aged below 500°C. On the contrary,

depletion of Ni from matrix with the formation of precipitates becomes dominant in increasing the transformation temperatures when the samples are aged at and above 500°C.

The transformation temperatures above 100°C were achieved with aging the samples above 550°C for 3 hours. Thus, aging at 550°C for 3 hours condition was selected for functional fatigue tests.

Normalized heat flow vs temperature curves of extruded $Ni_{50.3}Ti_{29.7}Hf_{20}$ and aged $Ni_{50.3}Ti_{29.7}Hf_{20}$ samples from DSC experiments are shown in Figure 4.1-2 and Figure 4.1-3, respectively. The corresponding transformation temperatures which are drawn from these curves are presented in Table 1. Mf temperature decreased from 33,2°C to 29°C, while Af temperature decreased from 109,9°C to 103°C at the end of the 3 stress free cycles for extruded sample. Beside this, M_s and A_s temperatures of extruded sample exhibited similar decreasing trend with the cycles.
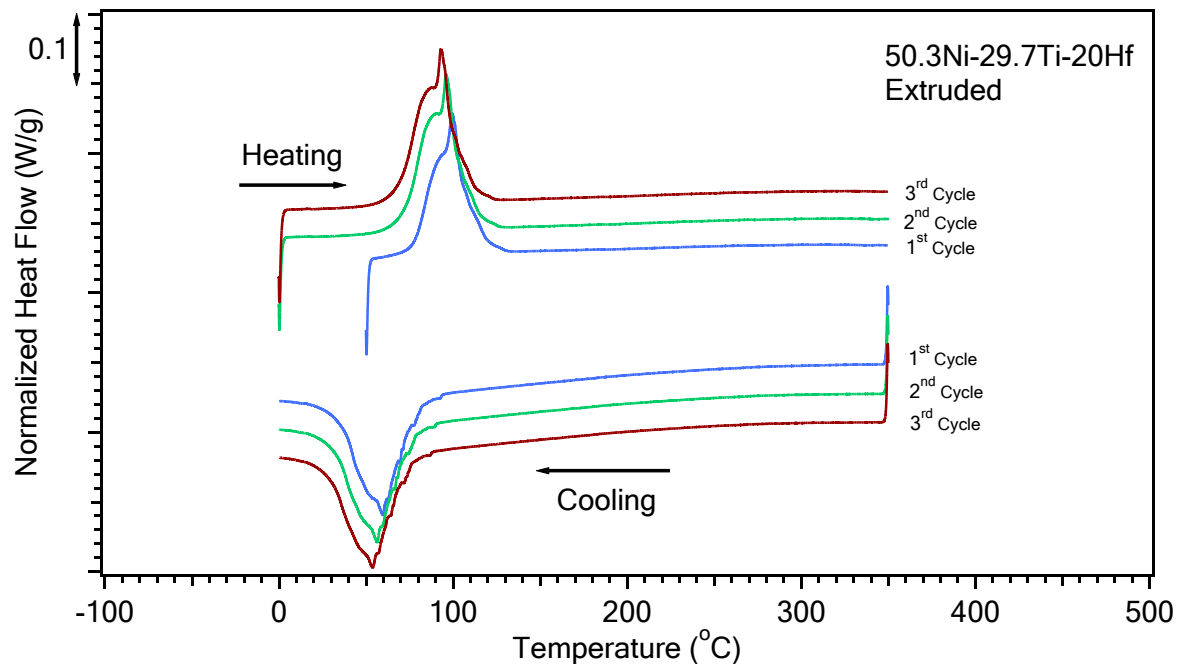
Figure 4.1-2. Normalized heat flow vs temperature curves of extruded $Ni_{50.3}Ti_{29.7}Hf_{20}$ sample.

On the other hand, aged samples showed excellent cyclic stability during stress free transformation temperature measurements. Transformation temperatures decreased between 1,7°C and 3°C at the end of the 3 cycles and this indicates perfect cyclic stability

in terms of transformation temperatures. Likewise, transformation temperatures were above the threshold value which is 100ºC for satisfying the condition of being HTSMA.
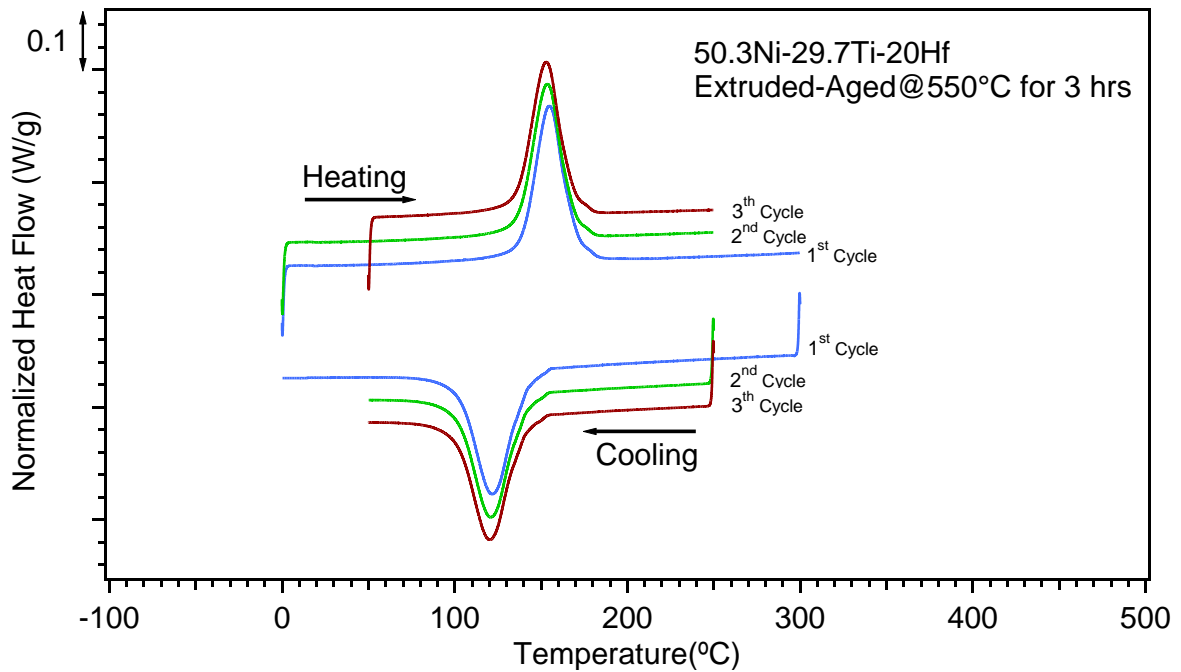
Figure 4.1-3 Normalized heat flow vs temperature curves of aged $Ni_{50.3}Ti_{29.7}Hf_{20}$

The comparison of the transformation temperatures of extruded and aged samples demonstrated the effect of aging on both transformation temperatures and cyclic stability (Table 4.1-1). Transformation temperatures of aged sample are above or close to 100ºC while extruded sample's transformation temperatures are below 100ºC. It is obvious that aging at 550ºC for 3 hours increases the transformation temperatures. It is also observed that cyclic stability of aged sample is better than that of the extruded sample.

Table 4.1-1 Transformation temperatures of extruded and aged $Ni_{50.3}Ti_{29.7}Hf_{20}$ samples which were drawn from the DSC curves.

Sample	Cycle	Transformation Temperatures (^0C)			
		M_f	M_s	A_s	A_f
Extruded	1	33.2	79.7	77.3	109.9
	2	30.2	78.2	70.4	106.5
	3	27	75.1	67	103.6
	Difference (^oC) (3-1)	-6.2	-4.6	-10.3	-6.3
Aged at 550^oC for 3 hours	1	100.9	142	137.7	171.3
	2	99.9	141.3	136.4	168.9
	3	99.2	139.8	135.4	168.3
	Difference (^oC) (3-1)	-1.7	-2.2	-2.3	-3

4.2 Load Biased Heating and Cooling

Figure 4.2-1 and Figure 4.2-2 represent the strain vs. temperature response under increasing constant stress levels for extruded and aged samples, respectively. Actuation and irrecoverable strain values were drawn from strain vs temperature curves and shown in Figure 4.2-3. Actuation strain increased when applied stress magnitudes were increased for both samples. Extruded sample showed irrecoverable strain under 300 MPa stress level, and fracture occurred during cooling period under 600 MPa. Aged sample showed irrecoverable strain under 600 MPa, however it did not fracture even under 600 MPa stress

magnitude. Stress level was not increased further for this sample. Actually, load biased experiments were done on $Ni_{50.3}Ti_{29.7}Hf_{20}$ alloy and the results were published previously in the literature, however, in this study load biased experiments were also conducted before the functional fatigue experiments to determine the threshold stress level at which irrecoverable strain was observed.
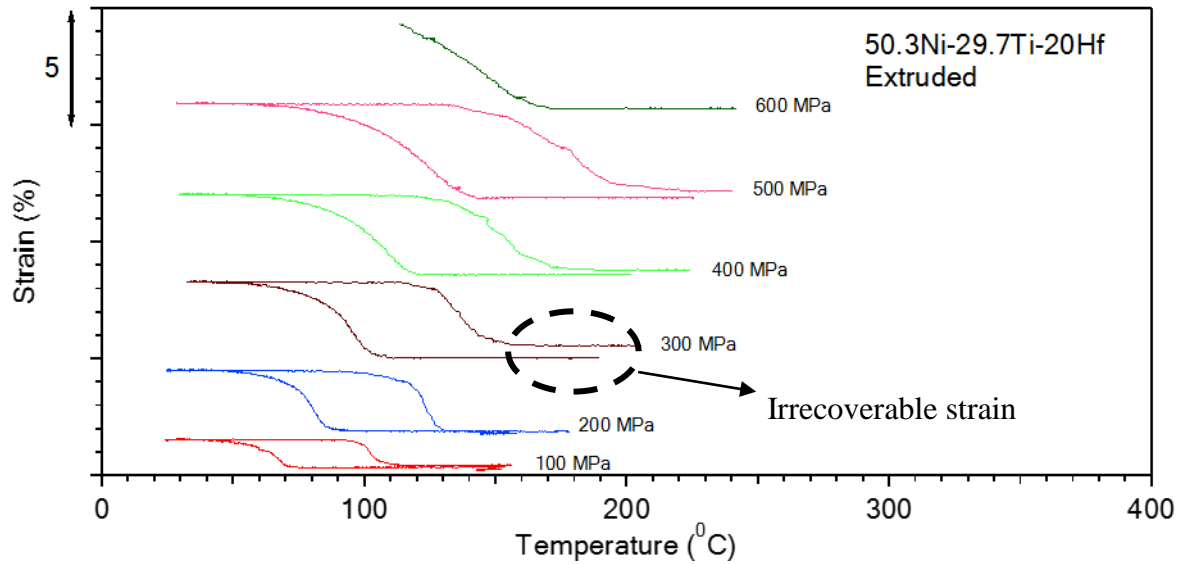
Figure 4.2-1 Strain vs Temperature curves of extruded $Ni_{50.3}Ti_{29.7}Hf_{20}$ sample under increasing constant stress magnitudes during isobaric heating-cooling experiments.

It is shown in Figure 4.2-1 that the irrecoverable strain appeared under 300 MPa constant stress level for the extruded sample. On the other hand, aged sample does not show noticeable irrecoverable strain up to 600 MPa. Therefore, the functional fatigue experiments were done under 200 MPa, which was the stress level that no irrecoverable strain was observed for both of the samples.

43
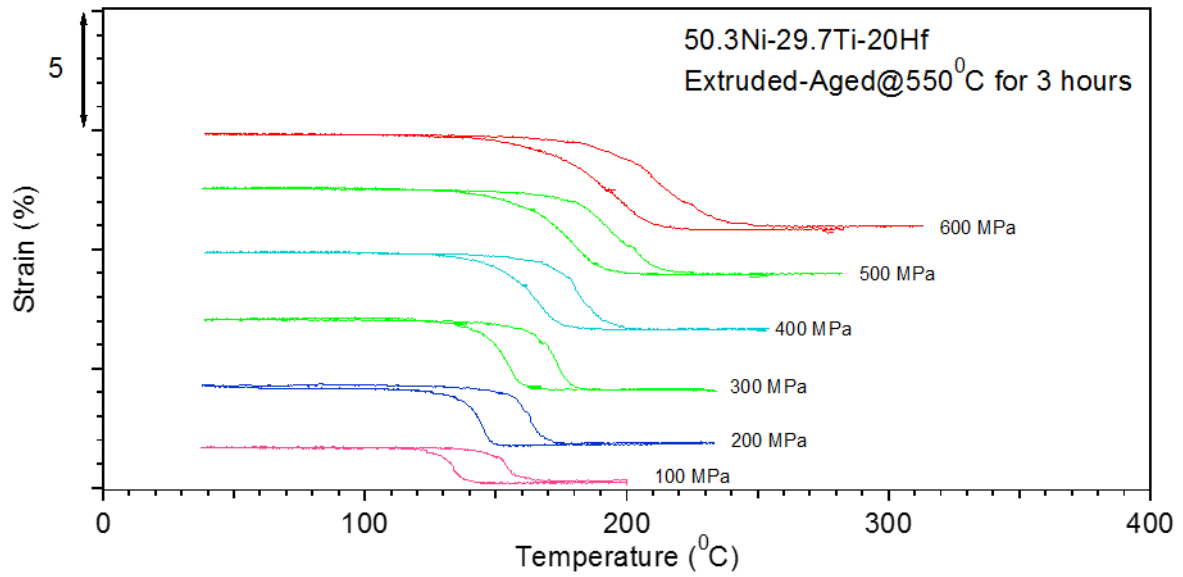
Figure 4.2-2 Strain vs Temperature curves of aged $Ni_{50.3}Ti_{29.7}Hf_{20}$ sample under increasing constant stress magnitudes during isobaric heating-cooling experiments.

Maximum irrecoverable strain magnitude was observed at 300 MPa on extruded sample (Figure 4.2-3). It was expected that magnitude of irrecoverable strain should be increased with the increase of the stress level. However, less irrecoverable strain was observed at the stress levels which were higher than 300 MPa. It can be explained with the increase in critical stress for slip with the plastic deformation via the applied stress. Since same sample was used for incremental load-biased heating and cooling tests (not virgin sample for each stress levels), plastic deformation at 300 MPa stress level might lead to an increase in critical stress for slip. Thus, sample might show less irrecoverable strain at higher stress levels. Also, transformation temperatures were increased with the increase in stress levels

16
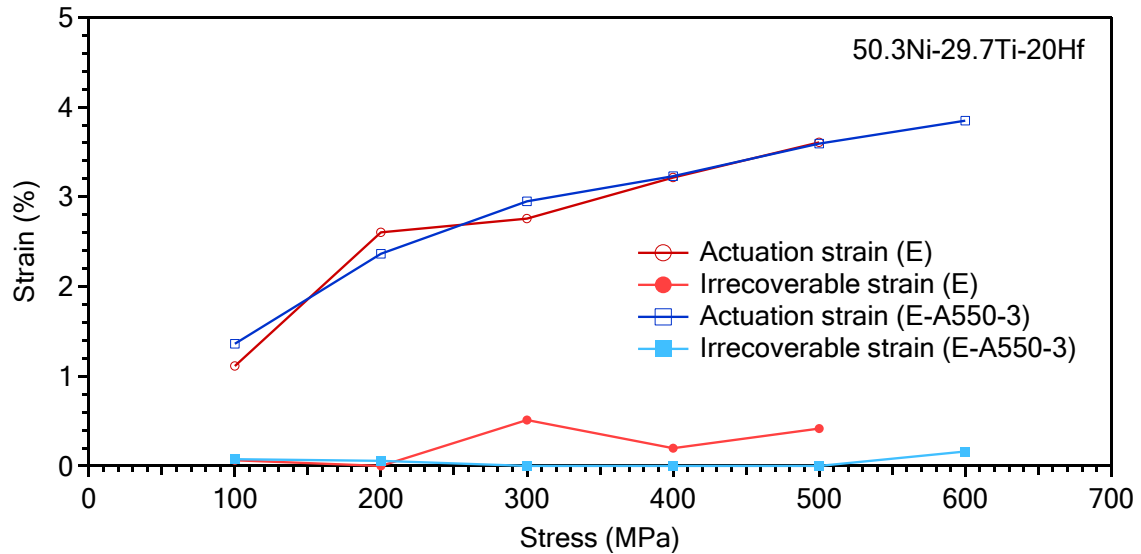
Figure 4.2-3 Actuation and irrecoverable strain values which were drawn from strain vs temperature curves of the isobaric heating-cooling experiments of extruded and aged $Ni_{50.3}Ti_{29.7}Hf_{20}$ samples.

It can be seen from Figure 4.2-3 that actuation strain increased with the increase in applied stress magnitudes for both of the samples. It is known that nano-sized precipitates are the main reasons of having less transforming volume in the matrix. Thus, lower actuation strains were expected for the aged samples in general. However, extruded sample showed less actuation strain for 100 MPa stress level. It is possible that 100 MPa stress level was not enough to activate the orientation of martensite variants through the most favorable one. For aged sample on the other hand, local stress fields around the precipitates could trigger the orientation of the more martensite variants through the most favorable one such that higher actuation strain value could be achieved.

For 200 MPa stress level, external load became dominant for variant reorientation and higher actuation strain was observed for extruded sample, since extruded sample has no nano-sized precipitates which strengthen the matrix. When the stress is increased to 300 MPa, actuation strain of extruded sample became lower than the actuation strain of aged sample. It must be noted that, irrecoverable strain was observed for extruded sample under 300 MPa stress level. Therefore, actuation strain was lower for extruded sample because of plastic deformation which could not be recovered. For the stress levels which were higher than 300 MPa, there could be some reasons of observing same recoverable strain values for extruded and aged samples. Firstly, irrecoverable strains which were observed at the extruded sample for stress levels higher than 300 MPa might result decrease in actuation

strain. Secondly, plastic strain which were induced to the sample at previous loading might increase the matrix strength. Thus, higher actuation strains may not be observed for extruded sample.

Speaking of irrecoverable strains, negligible irrecoverable strains were observed for 100 MPa stress level for both of the samples. For the stress levels between 200 MPa and 500 MPa, extruded sample showed irrecoverable strain where aged sample showed no irrecoverable strain. This can be explained as nano-sized precipitates strengthen the matrix in the aged sample and also increase the critical stress for slip. For 600 MPa stress level, aged sample showed minimal irrecoverable strain for the first time. However, extruded sample was fractured under 600 MPa. It is also an evidence that nano-sized precipitates strengthen the matrix.

4.3   Functional Fatigue Tests

Functional fatigue experiments were conducted under constant stress magnitude of 200 MPa since irrecoverable strain were first observed under 300 MPa in load biased heating-cooling experiment of the extruded sample. Therefore, 200 MPa stress magnitude was set as the threshold stress level. It has been already known that UCT has a negative effect on the fatigue life of HTSMAs from previous studies [18].When UCT increases, actuation strain of the sample increases since there are some local regions where heating to higher temperatures is necessary for further transformation of martensite to austenite. It should be noted that UCT is set to a temperature where it is sufficient for the complete austenitic transformation. However, there is an accumulation of dislocations in the matrix such that the increase in the dislocation density leads to an increase in the transformation temperatures due to the necessity of overheating for full austenitic transformation. If the UCT is higher, the sufficient overheating to overcome the dislocation barriers is supplied to achieve full transformation. The increase in UCT together with the full transformation along the sample is accompanied with an increase in actuation strain. Additionally, increase in actuation strain leads more expansion and contraction of cracks which promotes crack propagation. Other effect of UCT can be considered as decreasing the strength of the material at relatively higher temperatures, which results early failure. However, the effect of UCT was not the main focus in this study. The main aim of this thesis is the investigation of the effect of aging on the functional fatigue life of NiTiHf alloy [15].

Since the transformation temperatures of extruded and aged samples are different, determination of one constant UCT temperature for both extruded and aged samples is not feasible. Selecting UCT considering the austenite finish temperature of the aged samples to achieve complete austenitic transformation causes unnecessary heating of extruded sample, which leads early failure. On the other hand, selecting UCT considering the austenite finish temperature of the extruded samples to complete austenite formation causes an incomplete austenitic transformation for aged sample. Thus, the stress free transformation temperatures which were drawn from the DSC curves are considered to set the UCT temperatures in the functional fatigue experiments. As a summary, UCT was set to A_f + 130°C, considering A_f temperatures of the samples obtained from DSC experiments separately, which are approximately 240°C for the extruded sample and 300°C for the aged sample.

Strain vs. Temperatures responses, transformation temperatures, hysteresis and actuation strain magnitudes of the samples with the number of cycles from functional fatigue tests were investigated for some selected cycles, since samples were heated and cooled under constant stress magnitudes for thousands of cycles. The selected cycles from the experiments are given in Table 4.3-1.

Table 4.3-1. Investigated cycles for extruded and aged samples

	Samples	
	Extruded	Aged
	1	1
	100	100
	200	200
	500	500
Cycle number	1000	1000
	2000	2000
	5000 (last cycle)	5000
		7000
		10000
		13000
		16534 (last cycle)

An attention should be paid to early cycles because the shape memory properties of the alloys are stabilized with number of cycles. Thus, the investigation of the early cycles became more important to understand the cyclic stability of these materials. However, investigated cycles were selected same for extruded and aged samples, in sake of consistency.

Figure 4.3-1 represents the Strain vs Temperature response of extruded sample under 200 MPa, for different number of cycles. Extruded sample did not fracture until 5000th cycle. However, it lost its shape recovery characteristic through the selected temperature region and test was stopped. Lost in shape memory characteristic can be defined as lost in actuation strain. It should be noted that, the sample lost the characteristic shape recovery

transformation curve behavior after 1000th cycle, which makes impossible to determine the transformation temperatures and hysteresis. However, it continued to show very low actuation strain. Thus, transformation temperatures were not determined after 1000th cycle, but actuation strains were calculated.
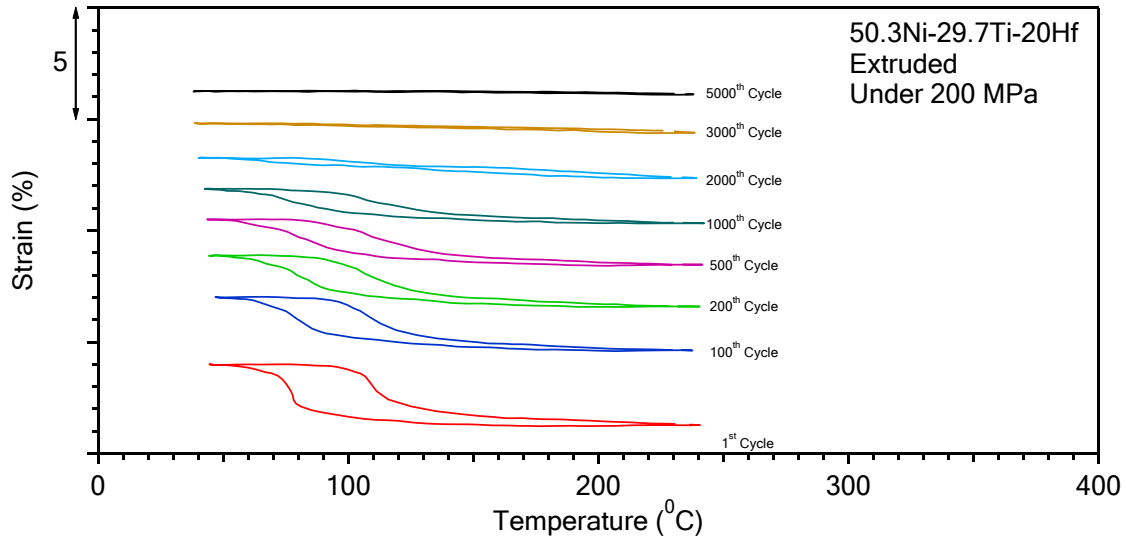
Figure 4.3-1. Strain vs Temperature Curves for Different Cycles for extruded Ni$_{50.3}$Ti$_{29.7}$Hf$_{20}$ sample

Figure 4.3-2 shows the evolution of transformation temperatures with respect to number of cycles of extruded sample under 200 MPa stress level. It can be seen that there was no noticeable change in the transformation temperatures for the first 1000 cycles. The evolution of the transformation temperatures is represented in Table 4.3. It can be concluded that M_f and A_s temperatures have a decreasing trend while A_f and M_s temperatures have an increasing trend.
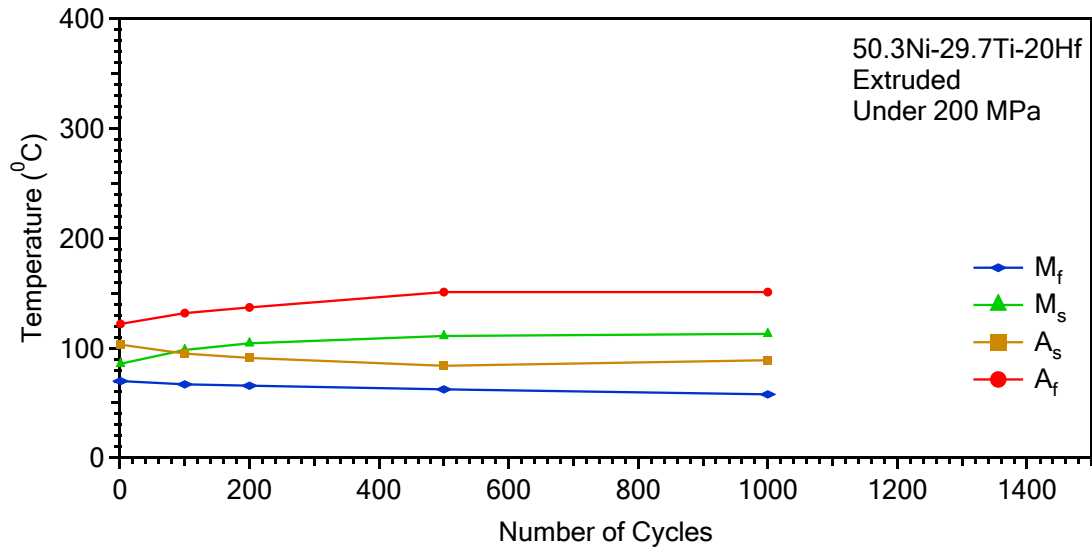
Figure 4.3-2. Change of Tranformation Temperatures with respect to Number of Cycles for extruded $Ni_{50.3}Ti_{29.7}Hf_{20}$

Table 4.3-1 Evolution of Tranformation Temperatures with respect to Number of Cycles for extruded $Ni_{50.3}Ti_{29.7}Hf_{20}$

	M_f		M_s		A_s		A_f	
	First	**Last**	**First**	**Last**	**First**	**Last**	**First**	**Last**
Temperature (ºC)	69.9	57.7	85.6	112.9	103.1	88.8	121.9	151
Difference (ºC) (Last – First)	-12.2		27.3		-14.3		29.7	

The change in hysteresis with respect to number of cycles for extruded sample under 200 MPa is represented in Figure 4.3-3. The initial value of the hysteresis was found as 35.1ºC and decreased down to 29.1ºC at the 200th cycle and started to increase until 1000th cycle up to 35.4ºC.

50
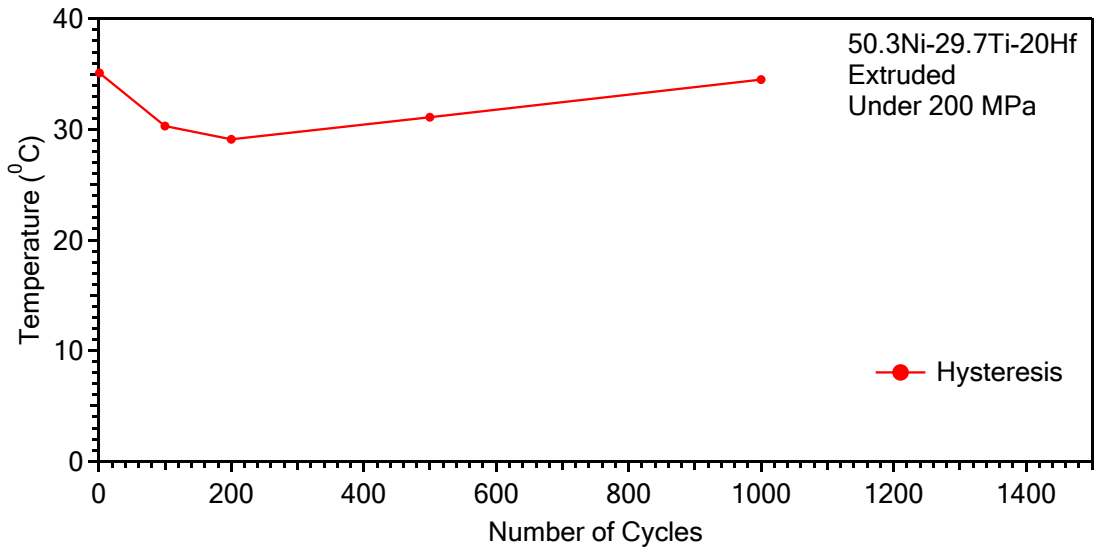
Figure 4.3-3. Change in Hysteresis of Extruded $Ni_{50.3}Ti_{29.7}Hf_{20}$ Sample Under 200 MPa

Figure 4.3-4 shows the evolution of the actuation strain with respect to number of cycles for the extruded sample under 200 MPa. The value of the actuation strain was 2.78% at the beginning and decreased to 0.18% at the end of the 5000th cycle.

Figure 4.3-4. Evolution of the actuation strain with respect to number of cycles for the extruded $Ni_{50.3}Ti_{29.7}Hf_{20}$ sample under 200 MPa

The Strain vs Temperature responses of the aged sample for different number of cycles under 200 MPa stress level are shown in Figure 4.3-5. Sample fractured at 16535th cycle, but it demonstrated actuation strain until the last cycle.
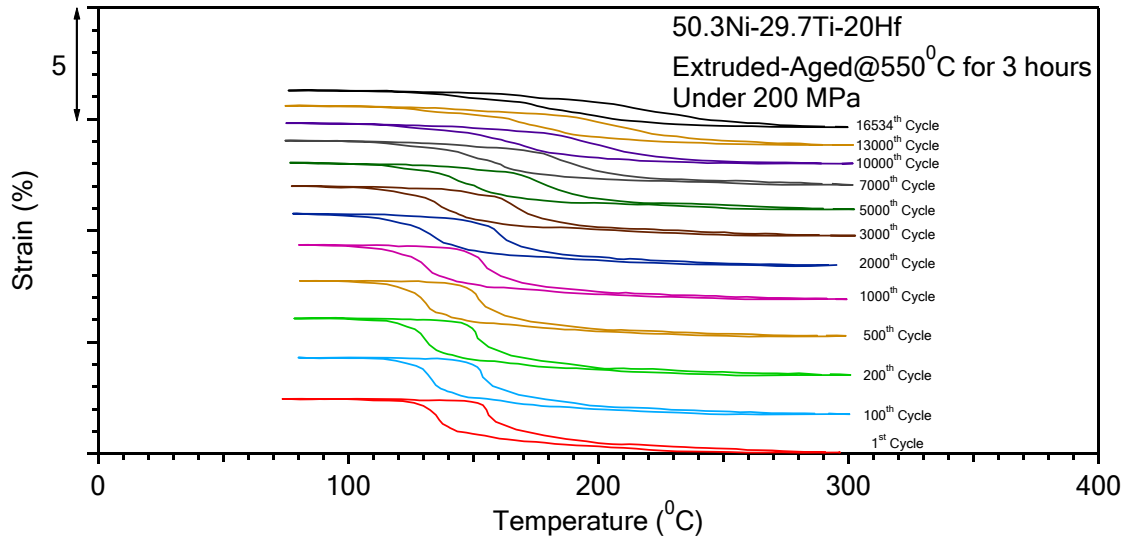
Figure 4.3-5. The Strain vs Temperature responses of the aged $Ni_{50.3}Ti_{29.7}Hf_{20}$ sample for different number of cycles under 200 MPa

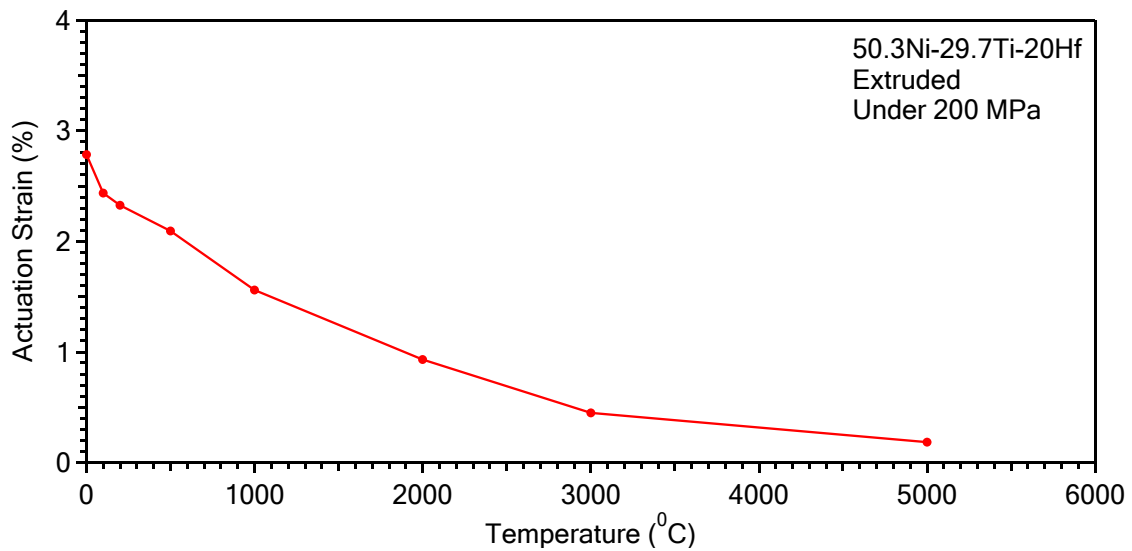The evolution of the transformation temperatures with respect to number of cycles for aged sample under 200 MPa stress level is presented in Figure 4.3-6. A small decrease for all transformation temperatures were observed through the first 500 cycles. Then, all transformation temperatures increased until the last cycle of the experiment.
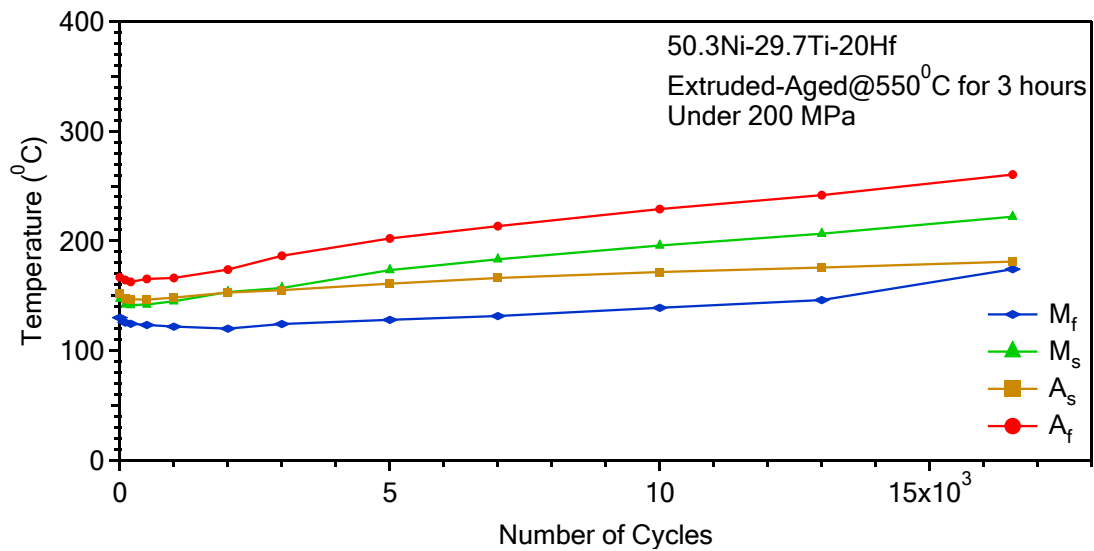
Figure 4.3-6. The evolution of the transformation temperatures with respect to number of cycles for aged $Ni_{50.3}Ti_{29.7}Hf_{20}$ sample under 200 MPa

Comparison of transformation temperatures which were drawn from the first and the last cycles of the functional fatigue experiments and the differences in the values are presented in Table 4.3-2 It can be concluded that, the highest increase in transformation temperatures was observed for A_f, while lowest increase was observed for A_s temperature.

Table 4.3-2 Comparison of Transformation temperatures of First and Last Cycles for aged $Ni_{50.3}Ti_{29.7}Hf_{20}$ sample

|	M_f		M_s		A_s		A_f	
Temperature (ºC)	**First**	**Last**	**First**	**Last**	**First**	**Last**	**First**	**Last**
	130	174.1	147.2	222	152.3	181	166.8	260.4
Difference (ºC) **(Last – First)**	44.1		74.8		28.7		93.6	

Figure 4.3-7 presents the thermal hysteresis evolution of the aged sample during the functional fatigue experiment under 200 MPa. The thermal hysteresis values of the aged sample under 200 MPa stress level drastically increased for the first 3000 cycles, then a slight increase was observed after that point until failure.
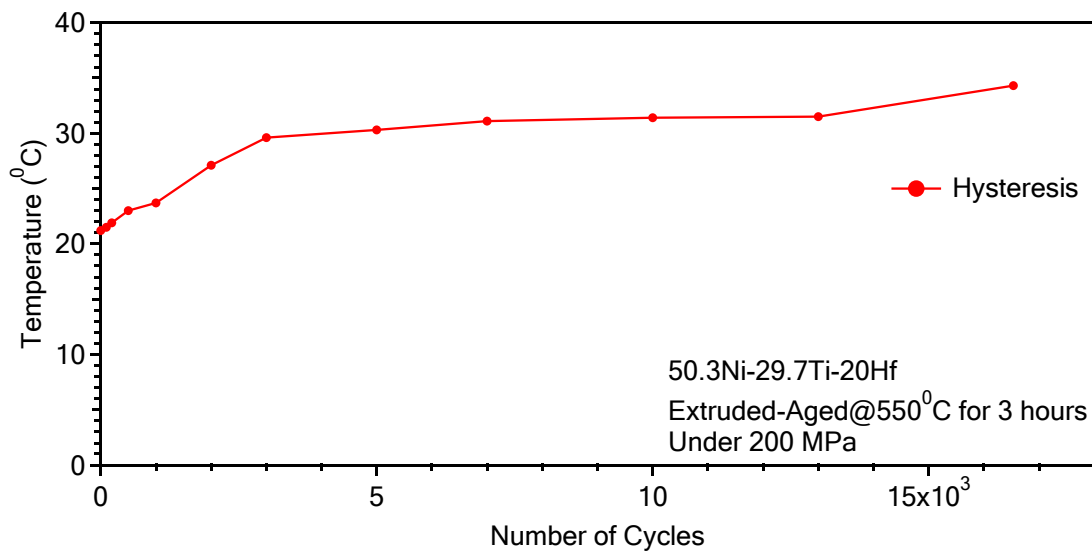
Figure 4.3-7. The thermal hysteresis evolution of the aged $Ni_{50.3}Ti_{29.7}Hf_{20}$ sample during the functional fatigue experiment under 200MPa

Figure 4.3-8. shows the change in actuation strain with respect to number of cycles for the aged sample under 200 MPa stress level. The initial value of sctuation strain was determined as 2.56% and increased up to 2.59% for the first 100 cycles, then decreased down to 1.66% at the end of the last cycle.
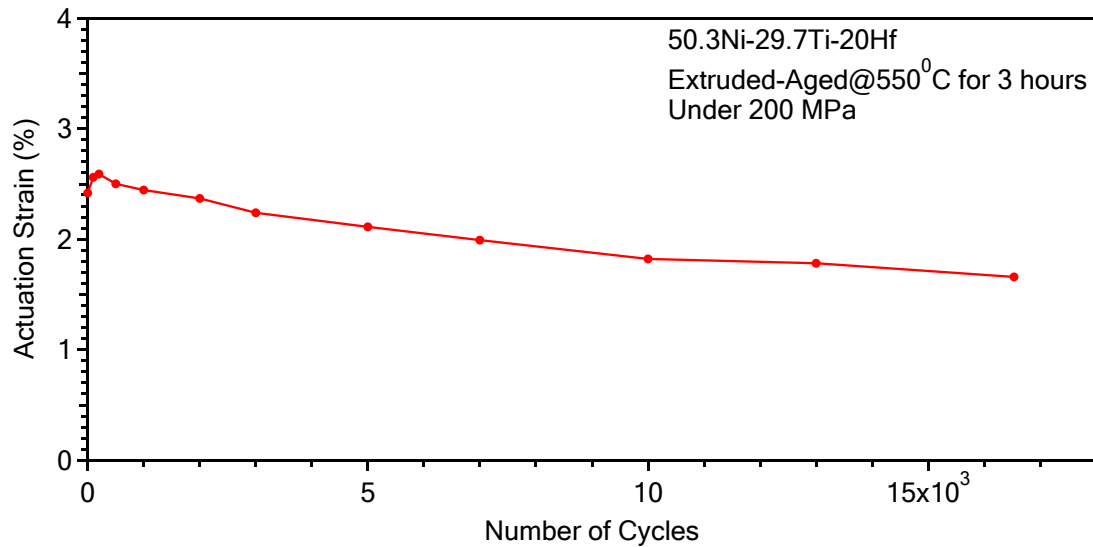
Figure 4.3-8. The change in actuation strain with respect to number of cycles for the aged sample under 200 MPa

Figure 4.3-9 represents the comparison of the change in transformation temperatures with the number of cycles for extruded and aged samples. Aged sample has higher transformation temperatures and thermal cyclic stability was maintained throughout the cycles. For better understanding, the evolution of transformation temperatures for the first 1000 cycles are plotted in Figure 4.3-10.
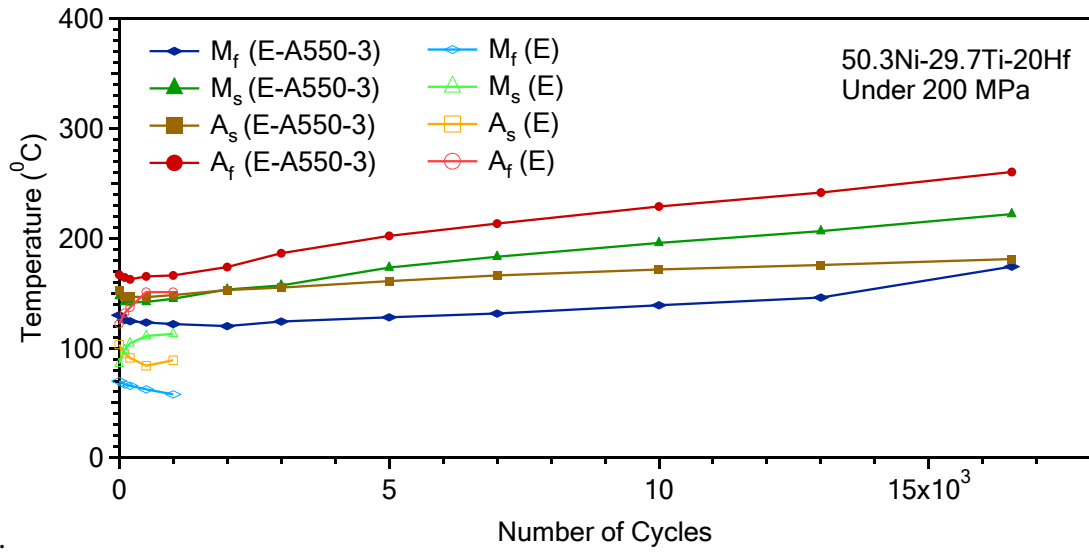
Figure 4.3-9. Comparison of the change in transformation temperatures with the number of cycles for extruded and aged samples
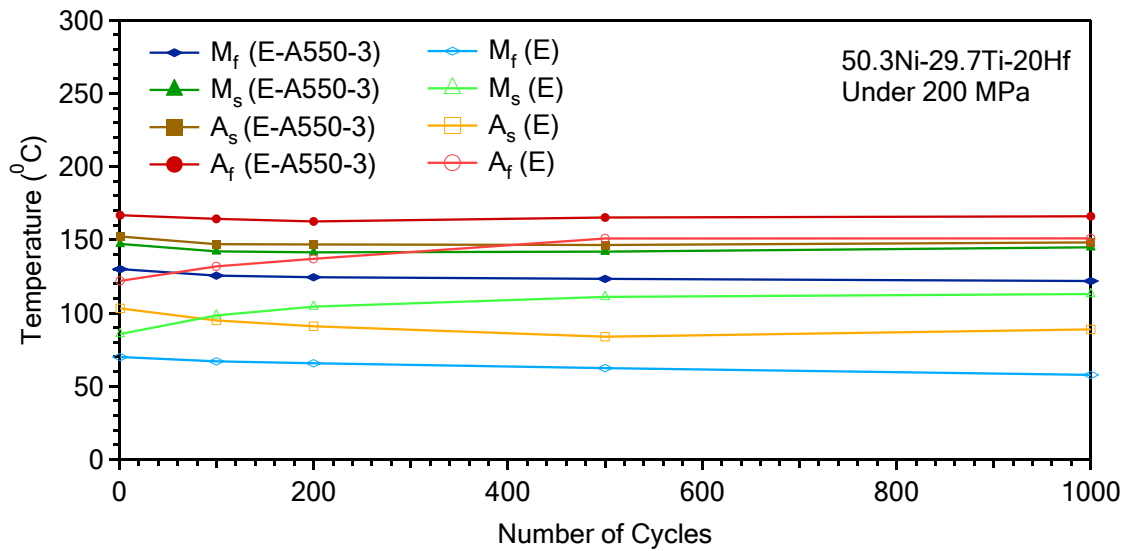
Figure 4.3-10. Evolution of transformation temperatures for the first 1000 cycles

The changes in the values of the transformation temperatures of the extruded and the aged samples for first 1000 cycles are listed at Table 4.3-3. Both samples showed same increasing and decreasing trend for the first 1000 cycles. However, aged sample showed excellent cyclic stability in terms of transformation temperatures since the change in transformation temperatures was below 10°C

Table 4.3-3 Transformation temperatures of the extruded and the aged samples for first 1000 cycle

		M_f		M_s		A_s		A_f	
		First	Last	First	Last	First	Last	First	Last
Temperature (ºC)	Extruded	69.9	57.7	85.6	112.9	103.1	88.8	121.9	151
	Aged	130	121.8	147.2	157	152.3	148.2	166.8	166.1
Difference (ºC)	Extruded	-12.2		27.3		-14.3		29.7	
(Last – First)	Aged	-8.2		9.8		-4.1		-0.7	

Figure 4.3-11 shows the comparison of thermal hysteresis response with respect to number of cycles for the extruded and aged samples. Aged sample showed lower hysteresis values than that of the extruded sample for the first 1000 cycles.

Figure 4.3-11. The comparison of thermal hysteresis response with respect to number of cycles for the extruded and aged samples
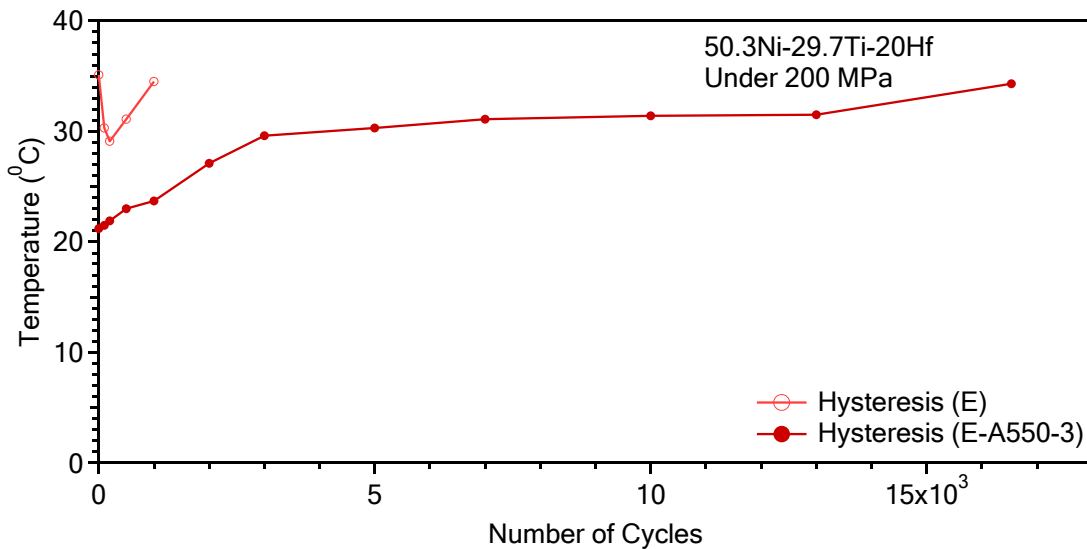
The evolution of the actuation strain with respect to number of cycles is represented in Figure 4.3-12 for both extruded and aged samples. It was determined that the extruded

sample demonstrated higher actuation strain than that of the aged sample. However, the actuation strain of the extruded samples decreased drastically down to 0.18% at the end of the 5000 cycle. On the other hand, aged sample showed better cyclic stability in terms of actuation strain which might be attributed to the increase in the strength with precipitation hardening mechanism.
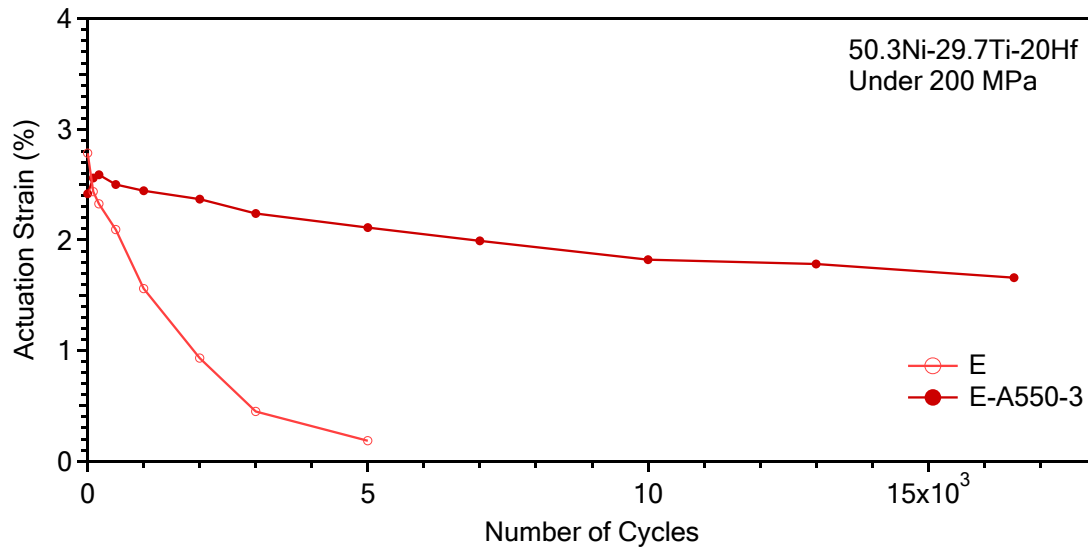
Figure 4.3-12. The evolution of the actuation strain with respect to number of cycles

4.4   Microstructural Investigation

4.4.1   Post-Mortem Optical Microscope Investiagtion

Figure 4.4-1 and Figure 4.4-2 show the optical microscope images of the extruded and the aged samples after functional fatigue tests, respectively. Micro cracks were observed in both of the samples. On the other hand, the cracks of the extruded sample are smaller than that of the aged samples. There is a possibility that the cracks did not propagate since extruded sample was exposed to lower cycle number due to losing the shape recovery behavior at the end of the 1000th cycle.
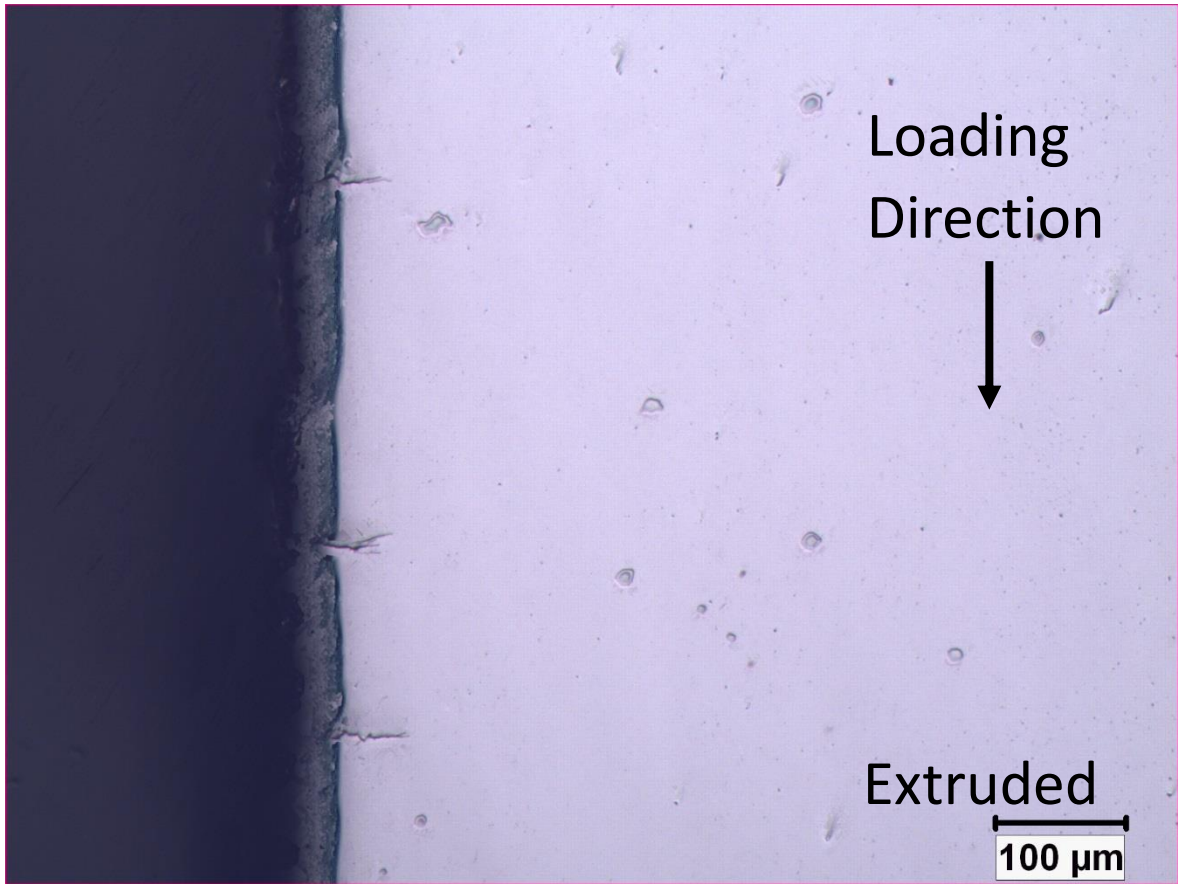
Figure 4.4-1. The optical microscope images of the extruded sample after Functional fatigue test

It is obvious that cracks were initiated from the surface and propagated during the functional fatigue experiments for both extruded and aged samples. One of the reasons of crack propagation might be the movement of martensite-austenite boundary. During the transformation, dislocation density increases because of this movement and the increase in the dislocation density leads to an increase in the residual stress and makes the material brittle such that the crack propagation becomes easier. Another reason of the crack propagation can be the inhomogeneity in temperature distributions. Since samples were cooled via forced air convection from the surface, midsection of the sample could not be cooled enough. Thus, midsection of the samples might be exposed to less temperature difference, such that volume percentage of the transforming area might decrease and this leads an incompatibility between the transforming regions throughout the section of the sample. Thus, the incompatibility in the matrix might ease the crack propagation as well.
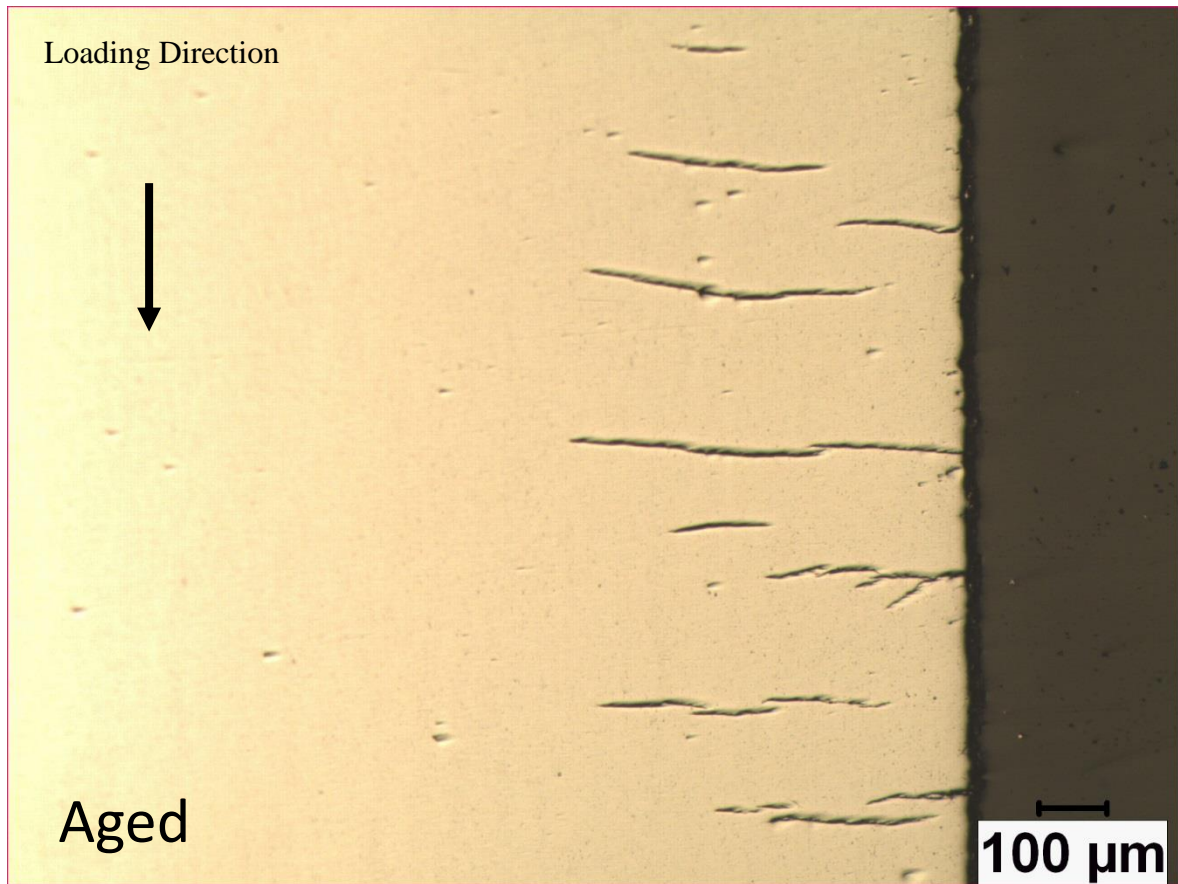
Figure 4.4-2. The optical microscope images of the aged sample after Functional fatigue test

Optical microscope images of the etched extruded and aged samples are presented in Figure 4.4-3 and Figure 4.4-4, respectively. Both samples were in martensitic structure. No retained austenite was observed under optical microscope and all structure was needle like martensitic structure. It can be conducted that austenite stabilization was not realized during functional fatigue tests. However, optical microscope studies are not enough for high resolution investigations such that further studies should be conducted using transmission electron microscope.

Figure 4.4-3. Optical microscope images of the etched extruded samples after functional fatigue test
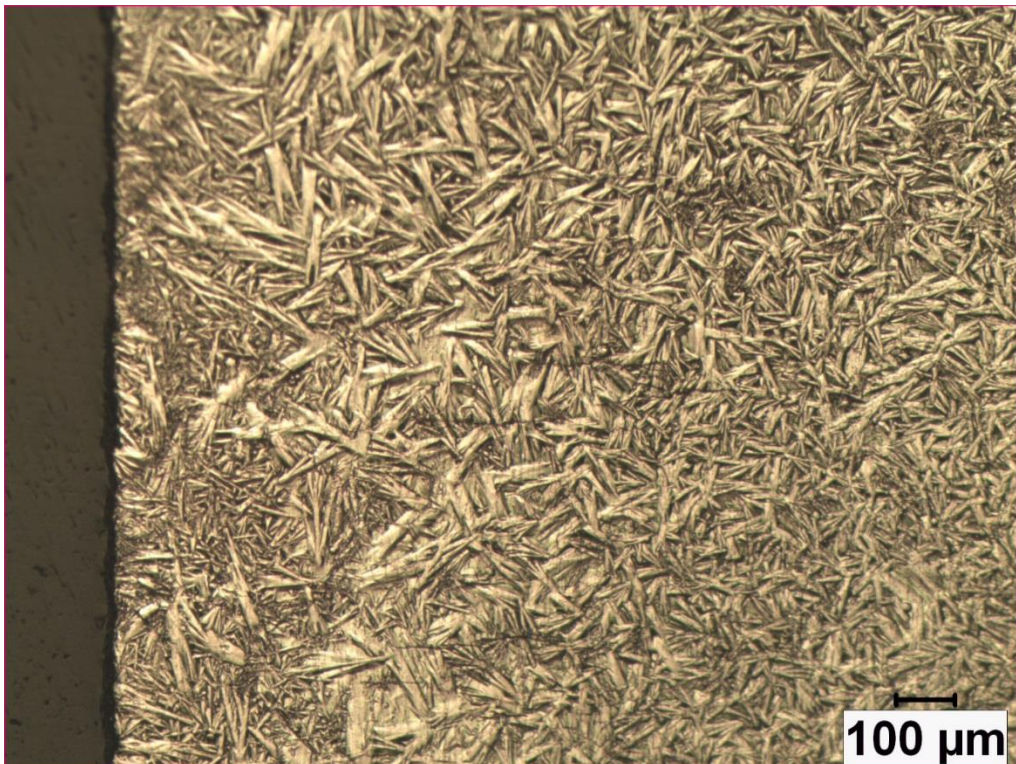
Figure 4.4-4. Optical microscope images of the etched aged samples after functional fatigue test

4.4.2   Transmission Electron Microscopy

Transmission Electron Microscopy studies were also conducted to reveal the twin structure in the extruded and the precipitate formation in the aged samples. The very common internal twin structure was determined in the extruded sample and shown in Figure 4.4-5. Very thin twinning formation was observed inside of the martensitic plates as expected from the previous microstructural studies in the literature.
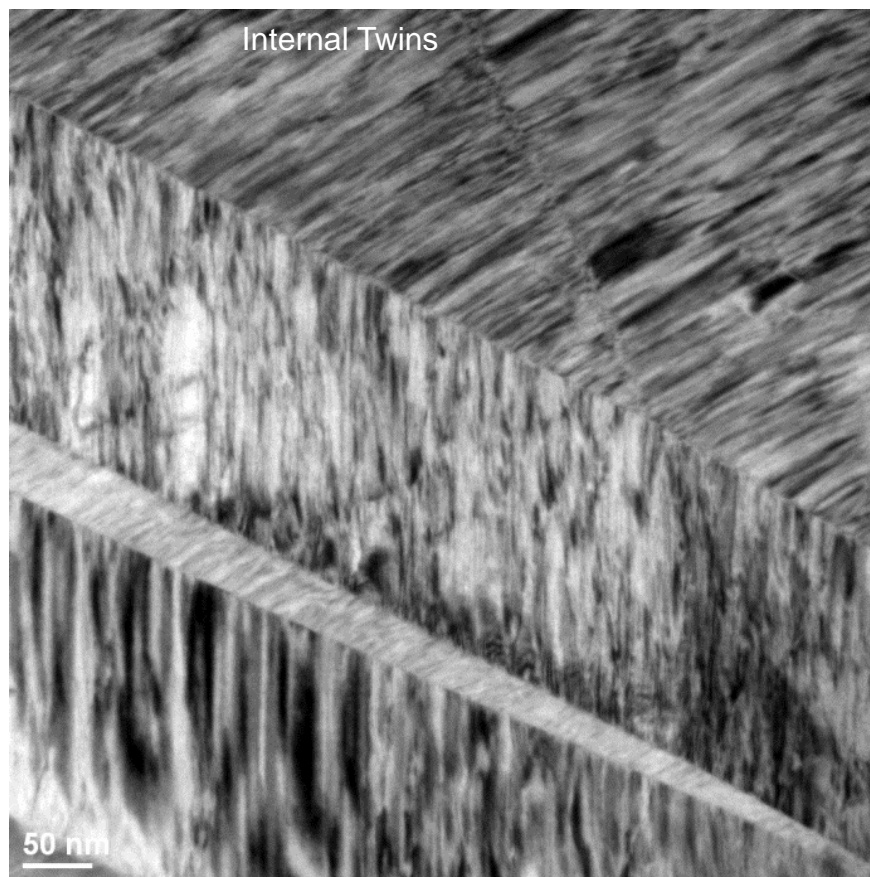
Figure 4.4-5. Internal twin structure was determined in the extruded sample

Ti_2NiHf (O) and HfO_2 oxide particles were observed in the aged sample from the TEM investigation, which can be seen in Fig 4.4-6. Electron Dispersive Spectroscopy (EDS) Analysis of the Ti_2NiHf(O) and HfO_2 oxide particles are presented at Table 4.4-1 and table 4.4-2, respectively. EDS analysis were done using the spectrometer which was attached to the TEM. Therefore, these results provided us more reliable values in terms of the chemistry of the particles.

Formation of these oxide particles could take place during production and processing of the materials. These precipitates were not equally distributed in the matrix. Therefore, they do not harden and increase the strength of the materials. They act like discontinuities in the matrix such that stress concentration around these particles might be the main reason of crack initiation and propagation. Moreover, this crack initiation and propagation lead the material to experience early failure during functional fatigue experiments.

Table 4.4-1 Elemental Analysis of Ti2NiHf

Element	Weight %	Atomic %
O(K)	2.94	13.42
Ti(K)	25.57	38.95
Ni(K)	22.08	27.44
Hf(L)	49.39	20.18
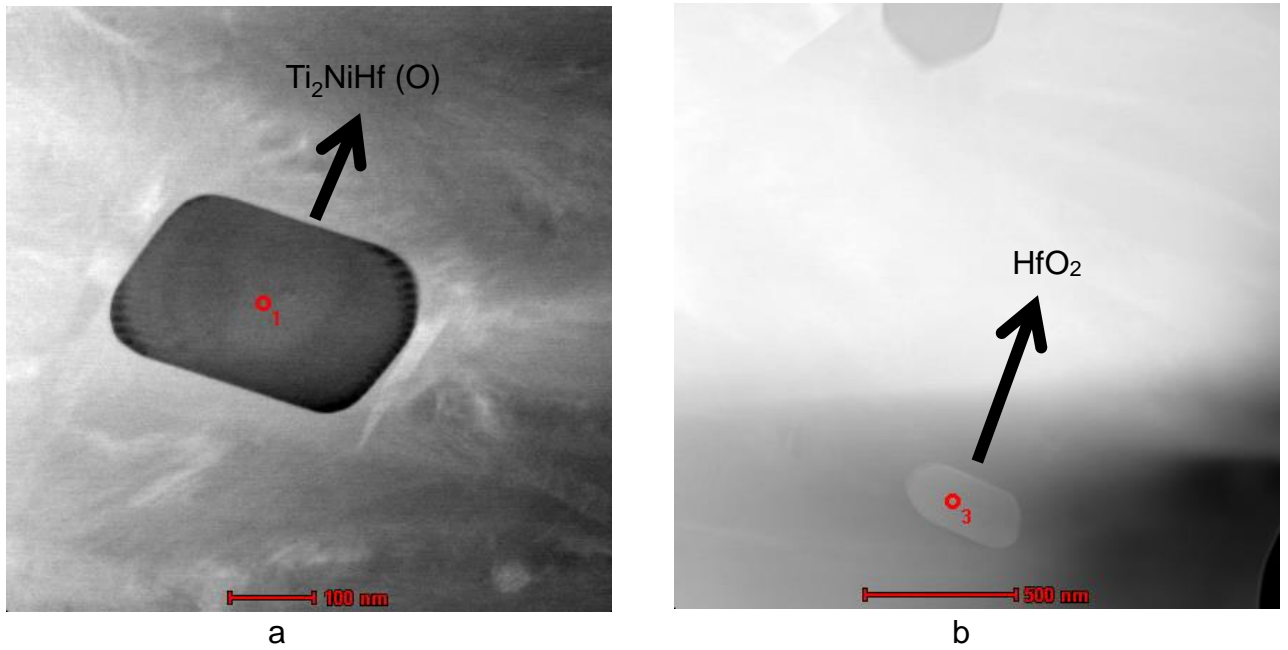
Figure 4.4-6. Oxide Particles a) Ti_2NiHf b)HfO

Table 4.4-2 Elemental Analysis of HfO

Element	Weight %	Atomic %
O(K)	14.80	65.97
Ti(K)	0.00	0.00
Ni(K)	0.00	0.00
Hf(L)	85.19	34.02

It has been already known from the literature that very well distributed H-phase nano-sized precipitates are the main reasons in the strength increase and the improvement of the shape memory properties of Ni-rich NiTiHf alloys. Therefore, it was important to determine the H-phase precipitates in the matrix after the aging process. It was found that there is a homogeneous distribution of H-phase nanostructured precipitates in the matrix as can be

seen in Figure 4.4-7 for the aged sample. The high resolution TEM image also showed that the size of the precipitates could be even at around 10nm.
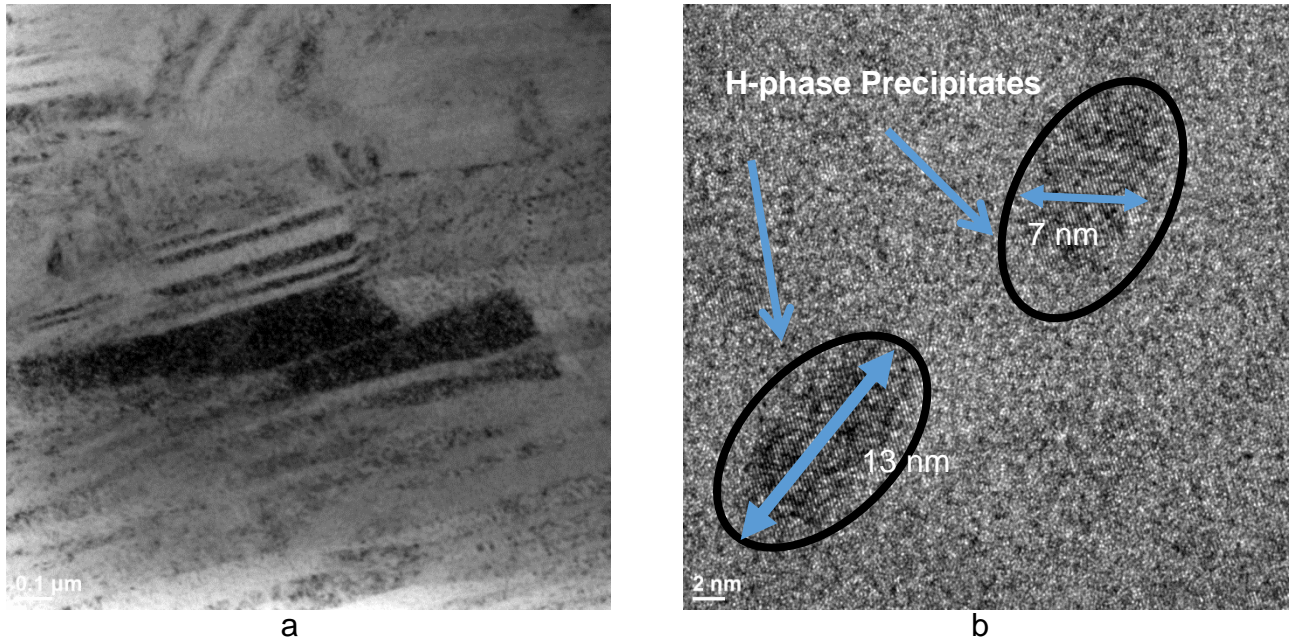
Figure 4.4-7. H Phase Precipitations

5 CONCLUSION

The conclusions which can be drawn from this study under the light of the all aforementioned results are presented below:

Load-biased heating and cooling tests revealed that aging 550°C for 3 hours led to a decrease in irrecoverable strain values, comparing to values acquired from the extruded sample. The irrecoverable strain was first detected in the aged sample under 600 MPa stress level. On the other hand, extruded sample showed irrecoverable strain under 300 MPa stress level during load-biased heating-cooling experiments. This can be explained with the increase in the strength of the alloy via the formation of nano-sized precipitates during aging process. The nano-sized precipitates block the dislocation motion and increase the strength of matrix. This increase led to an increase in the critical stress for slip. Thus, irrecoverable strains related with the plastic deformation were not observed until 600 MPa stress level for the aged sample.

It is obvious that aging has a positive effect on the cyclic stability in terms of both transformation temperatures and actuation strain during functional fatigue tests. Drastic increase in transformation temperatures and a noticeable decrease in actuation stain values of extruded sample can be explained with the accumulation of dislocations during the martensite-austenite transformation under constant stress magnitudes. In the absence of nano-scale precipitates, extruded sample exhibited more actuation strain under 200 MPa in the functional fatigue experiments during the initial cycles. However, higher transforming region which is the reason of having higher actuation strain leads to the formation of more dislocation and accumulation of dislocation in the matrix throughout the cycles. The increase in dislocation density mitigates the thermal and thermo-mechanical cyclic stability of these alloys. However, nano-scale precipitates in the matrix of the aged sample act as barriers to the dislocation motions. Less dislocation movement leads to less dislocation accumulation. Thus, cyclic stability of the aged sample is better than that of the as extruded sample.

The TEM analysis reveals that there were TiNiHf and Hf oxide particles in the matrix. Since the oxide particles were not compatible with the structure of the matrix, they might act as stress concentrators such that crack initiation and propagation may become easier with the number of cycles in the functional fatigue experiments. Therefore, it is very

important to produce NiTiHf shape memory alloys via inhibiting the oxidation not only during casting but also during the secondary treatment processes.

It is the first study that compares the functional fatigue behavior of $Ni_{50,3}Ti_{29,7}Hf_{20}$ aged at $550^{o}C$ for 3 hours and as extruded HTSMAs in literature. Further studies can be focused on the effect of different aging temperatures for $Ni_{50,3}Ti_{29,7}Hf_{20}$ HTSMA on functional fatigue behavior of $Ni_{50,3}Ti_{29,7}Hf_{20}$.

REFERENCES

[1]   Otsuka, K. and Ren, X., Physical metallurgy of Ti-Ni-based shape memory alloys, *Progress in Materials Science*, vol. 50, no. 5, 511–678, **2005**.

[2]   Kockar, B., Karaman, I., Kim, J. I., Chumlyakov, Y. I., Sharp, J., and Yu, C. J. (Mike., Thermomechanical cyclic response of an ultrafine-grained NiTi shape memory alloy, *Acta Materialia*, vol. 56, no. 14, 3630–3646, **2008**.

[3]   Kockar, B., Karaman, I., Kulkarni, A., Chumlyakov, Y., and Kireeva, I. V., Effect of severe ausforming via equal channel angular extrusion on the shape memory response of a NiTi alloy, *Journal of Nuclear Materials*, vol. 361, no. 2–3 SPEC. ISS., 298–305, **2007**.

[4]   Ma, J., Karaman, I., and Noebe, R. D., High temperature shape memory alloys, *International Materials Reviews*, vol. 55, no. 5, 257–315, **2010**.

[5]   Kockar, B. *et al.*, Role of severe plastic deformation on the cyclic reversibility of a Ti 50.3Ni33.7Pd16 high temperature shape memory alloy, *Acta Materialia*, vol. 58, no. 19, 6411–6420, **2010**.

[6]   Santamarta, R. *et al.*, TEM study of structural and microstructural characteristics of a precipitate phase in Ni-rich Ni-Ti-Hf and Ni-Ti-Zr shape memory alloys, *Acta Materialia*, vol. 61, no. 16, 6191–6206, **2013**.

[7]   Kockar, B., Karaman, I., Kim, J. I., and Chumlyakov, Y., A method to enhance cyclic reversibility of NiTiHf high temperature shape memory alloys, *Scripta Materialia*, vol. 54, no. 12, 2203–2208, **2006**.

[8]   Meng, X. L., Zheng, Y. F., Wang, Z., and Zhao, L. C., Shape memory properties of the Ti36Ni49Hf15 high temperature shape memory alloy, *Materials Letters*, vol. 45, no. 2, 128–132, **2000**.

[9]   Karaca, H. E., Acar, E., Tobe, H., and Saghaian, S. M., NiTiHf-based shape memory alloys, *Materials Science and Technology*, vol. 30, no. 13, 1530–1544, **2014**.

[10]   Evirgen, A., Karaman, I., Santamarta, R., Pons, J., and Noebe, R. D., Microstructural characterization and shape memory characteristics of the Ni50.3Ti34.7Hf15shape memory alloy, *Acta Materialia*, vol. 83, 48–60, **2015**.

[11] Meng, X. L., Cai, W., Fu, Y. D., Li, Q. F., Zhang, J. X., and Zhao, L. C., Shape-memory behaviors in an aged Ni-rich TiNiHf high temperature shape-memory alloy, *Intermetallics*, vol. 16, no. 5, 698–705, **2008**.

[12] Evirgen, A., Basner, F., KAraman, I., Noebe, R. D., Pons, J., and Santamarta, R., Effect oF Aging on the Martensitic Transformation Characteristic of a Ni -Rich NiTiHf High Temperature Shape Memeory Alloy, *Functional Materials Letters*, vol. 05, no. 04, 1250038, **2012**.

[13] Karaca, H. E. *et al.*, Effects of nanoprecipitation on the shape memory and material properties of an Ni-rich NiTiHf high temperature shape memory alloy, *Acta Materialia*, vol. 61, no. 19, 7422–7431, **2013**.

[14] Benafan, O. *et al.*, Mechanical and functional behavior of a Ni-rich Ni50.3Ti29.7Hf20high temperature shape memory alloy, *Intermetallics*, vol. 50, 94–107, **2014**.

[15] Padula, S. *et al.*, Effect of upper-cycle temperature on the load-biased, strain-temperature response of NiTi, *Metallurgical and Materials Transactions A: Physical Metallurgy and Materials Science*, vol. 43, no. 12, 4610–4621, **2012**.

[16] Saghaian, S. M., Karaca, H. E., Souri, M., Turabi, A. S., and Noebe, R. D., Tensile shape memory behavior of Ni50.3Ti29.7Hf20high temperature shape memory alloys, *Materials and Design*, vol. 101, 340–345, **2016**.

[17] Bigelow, G. S., Garg, A., Padula, S. A., Gaydosh, D. J., and Noebe, R. D., Load-biased shape-memory and superelastic properties of a precipitation strengthened high-temperature Ni50.3Ti29.7Hf20alloy, *Scripta Materialia*, vol. 64, no. 8, 725–728, **2011**.

[18] Karakoc, O. *et al.*, Effects of upper cycle temperature on the actuation fatigue response of NiTiHf high temperature shape memory alloys, *Acta Materialia*, vol. 138, 185–197, **2017**.

[19] Mohd Jani, J., Leary, M., Subic, A., and Gibson, M. A., A review of shape memory alloy research, applications and opportunities, *Materials & Design (1980-2015)*, vol. 56, 1078–1113, **2014**.

[20] Song, G., Ma, N., and Li, H.-N., Applications of shape memory alloys in civil structures, *Engineering Structures*, vol. 28, no. 9, 1266–1274, **2006**.

[21] Araki, Y. *et al.*, *Potential of superelastic Cu–Al–Mn alloy bars for seismic applications*, vol. 40. **2011**.

[22] Maruyama, T. and Kubo, H., 12 - Ferrous (Fe-based) shape memory alloys (SMAs): properties, processing and applications BT - Shape Memory and Superelastic Alloys, in *Woodhead Publishing Series in Metals and Surface Engineering*, Woodhead Publishing, **2011**, 141–159.

[23] C. Lagoudas, D., *Shape memory alloys. Modeling and engineering applications. Papers based on the presentations at the 1st annual workshop on multifunctional nanomaterials, Red River, NM, USA, March 13–16, 2006*, vol. 1. **2008**.

[24] Khalil-Allafi, J., Dlouhy, A., and Eggeler, G., Ni4Ti3-precipitation during aging of NiTi shape memory alloys and its influence on martensitic phase transformations, *Acta Materialia*, vol. 50, no. 17, 4255–4274, **2002**.

[25] Radi, A., Khalil-Allafi, J., Etminanfar, M. R., Pourbabak, S., Schryvers, D., and Amin-Ahmadi, B., Influence of stress aging process on variants of nano-Ni4Ti3 precipitates and martensitic transformation temperatures in NiTi shape memory alloy, *Materials & Design*, vol. 142, 93–100, **2018**.

[26] Brno, D. H., On the precipitation in NiTi based shape memory alloys, no. April 2005, **2005**.

[27] Bucsek, A. N., Hudish, G. A., Bigelow, G. S., Noebe, R. D., and Stebner, A. P., Composition, Compatibility, and the Functional Performances of Ternary NiTiX High-Temperature Shape Memory Alloys, *Shape Memory and Superelasticity*, vol. 2, no. 1, 62–79, **2016**.

[28] Monroe, J. A., Gehring, D., Karaman, I., Arroyave, R., Brown, D. W., and Clausen, B., Tailored thermal expansion alloys, *Acta Materialia*, vol. 102, 333–341, **2016**.

[29] Atli, K. C., Karaman, I., Noebe, R. D., Bigelow, G., and Gaydosh, D., Work production using the two-way shape memory effect in NiTi and a Ni-rich NiTiHf high-temperature shape memory alloy, *Smart Materials and Structures*, vol. 24, no. 12, **2015**.

[30] Sehitoglu, H., Wu, Y., and Patriarca, L., Shape memory functionality under multi-cycles in NiTiHf, *Scripta Materialia*, vol. 129, 11–15, **2017**.

[31] Wu, Y. *et al.*, Shape Memory Response of Polycrystalline NiTi12.5Hf Alloy:

Transformation at Small Scales, *Shape Memory and Superelasticity*, vol. 1, no. 3, 387–397, **2015**.

[32] Abuzaid, W. and Sehitoglu, H., Functional fatigue of Ni50.3Ti25Hf24.7– Heterogeneities and evolution of local transformation strains, *Materials Science and Engineering A*, vol. 696, no. December 2016, 482–492, **2017**.

[33] Potapov, P. L., Shelyakov, A. V, Gulyaev, A. A., Svistunov, E. L., Matveeva, N. M., and Hodgson, D., Effect of Hf on the structure of Ni-Ti martensitic alloys, *Materials Letters*, vol. 32, no. 4, 247–250, **1997**.

[34] Besseghini, S., Villa, E., and Tuissi, A., Ni-Ti-Hf shape memory alloy: effect of aging and thermal cycling, *Materials Science and Engineering: A*, vol. 273–275, 390–394, **1999**.

[35] Meng, X. L., Cai, W., Chen, F., and Zhao, L. C., Effect of aging on martensitic transformation and microstructure in Ni-rich TiNiHf shape memory alloy, *Scripta Materialia*, vol. 54, no. 9, 1599–1604, **2006**.

[36] Firstov, G. S., Van Humbeeck, J., and Koval, Y. N., High-temperature shape memory alloys: Some recent developments, *Materials Science and Engineering: A*, vol. 378, no. 1, 2–10, **2004**.

[37] Calhoun, C., Actuation Fatigue of Shape Memory Alloys, Texas A&M University, **2012**.

[38] Agboola, B. O. and Hartl, D. J., A STUDY OF ACTUATION FATIGUE OF SHAPE MEMORY ALLOY, *Proceedings of the ASME 2012 Conference on Smart Materials, Adaptive Structures and Intelligent Systems*, 1–7, **2017**.

CURRICULUM VITAE

Credentials

Name, Surname: Hasan Hüseyin Saygılı

Place of Birth: Sinanpaşa, Afyonkarahisar

Marital Status: Single

E-mail: hasan.h.saygili@gmail.com

Adress: Prof. Dr. Ahmet Taner Kışlalı Mah. 2903. Sok. İller Sitesi No:1/8 Çankaya/Ankara

Education

B.Sc. : Hacettepe University Mechanical Engineering Department Automotive Engineering Program (2009/2015)

M.Sc. : Hacettepe University Mechanical Engineering Department (2015/2018)

Foreign Languages

English

German

Work Experiences

Turkish Aerospace Industries, Inc. – Rotary Wing Technology Center (2018/-)

Hacettepe Technopolis Teknology Transfer Center - R&D Engineer (2015/2018)

Areas of Experiences

Shape Memory Alloys, Microstructure Engineering, Design Engineering

Projects and Budgets

TAI DKTM 2015/10 Project

Publications

-

Oral and Poster Presentations

Hasan H. Saygili, H. Onat Tugrul, Benat Kockar. "Investigating The Effect Of Aging Heat Treatment On The Functional Fatigue Behavior Of Ni50.3Ti29.7Hf20 High Temperature Shape Memory Alloy" *HTSMA 2018* May 15-18 Kloster Irsee, Germany

HACETTEPE UNIVERSITY
GRADUATE SCHOOL OF SCIENCE AND ENGINEERING
THESIS/DISSERTATION ORIGINALITY REPORT

HACETTEPE UNIVERSITY
GRADUATE SCHOOL OF SCIENCE AND ENGINEERING
TO THE DEPARTMENT OF MECAHNICAL ENGINEERING

Date: 10/07/2018

Thesis Title / Topic: The Development of a Fatigue Test Machine to Investigate the Functional Fatigue Life of High Temperature Shape Memory Alloys and The Determination of The Functional Fatigue Life of These Alloys

According to the originality report obtained by ~~myself~~/my thesis advisor by using the *Turnitin* plagiarism detection software and by applying the filtering options stated below on 09/07/2018 for the total of ....54...... pages including the a) Title Page, b) Introduction, c) Main Chapters, d) Conclusion sections of my thesis entitled as above, the similarity index of my thesis is ...8... %.

Filtering options applied:
1. Bibliography/Works Cited excluded
2. Quotes ~~excluded~~ / included
3. Match size up to 5 words excluded

I declare that I have carefully read Hacettepe University Graduate School of Sciene and Engineering Guidelines for Obtaining and Using Thesis Originality Reports; that according to the maximum similarity index values specified in the Guidelines, my thesis does not include any form of plagiarism; that in any future detection of possible infringement of the regulations I accept all legal responsibility; and that all the information I have provided is correct to the best of my knowledge.

I respectfully submit this for approval.

10/07/2018
H. Saygılı
Date and Signature

Name Surname: Hasan Hüseyin SAYGILI
Student No: N14325209
Department: Mechanical Engineering
Program: Materials and Manufacturing
Status: ☒ Masters   ☐ Ph.D.   ☐ Integrated Ph.D.

ADVISOR APPROVAL

APPROVED.

ASSOC. PROF. DR. BENAT KOÇKAR

B. Koçkar

(Title, Name Surname, Signature)